# NATIONAL ADVISORY COMMITTEE FOR AERONAUTICS

**TECHNICAL NOTE 2589**

## AN ANALYTICAL INVESTIGATION USING AERODYNAMIC LIMITATIONS OF SEVERAL DESIGNS OF HIGH STAGE PRESSURE RATIO MULTISTAGE COMPRESSORS

By Charles H. Voit and Arthur R. Thomson

Lewis Flight Propulsion Laboratory
Cleveland, Ohio

Washington
December 1951

NATIONAL ADVISORY COMMITTEE FOR AERONAUTICS

TECHNICAL NOTE 2589

# AN ANALYTICAL INVESTIGATION USING AERODYNAMIC LIMITATIONS OF SEVERAL DESIGNS OF HIGH STAGE PRESSURE RATIO MULTISTAGE COMPRESSORS

By Charles H. Voit and Arthur R. Thomson



## SUMMARY

An analysis of the effect of principal design variables on the stagewise design-point characteristics of multistage axial-flow compressors was made in order to determine whether the average stage pressure ratios of present-day commercial compressors can be raised. The investigation considers certain design limits and the manner in which these limits are affected by the principal design variables of an inlet stage, a typical intermediate stage, and a typical final stage of a multistage axial-flow compressor. Two velocity diagrams were investigated, the wheel plus vortex and the symmetrical at all radii diagrams. The optimum stagewise variations of axial velocity and relative inlet-air angle are determined. An analysis was made to estimate the possible over-all compressor pressure ratio for several stagewise distributions of these variables. The investigation indicates that for the wheel-plus-vortex velocity diagram and procedure followed, the axial velocity should increase stagewise through the compressor and the relative inlet-air angle should be lower in the later stages than in the inlet stage in order to produce the highest over-all total-pressure ratio for a given set of design conditions.

Two types of velocity diagram for the inlet stage were analyzed to determine which would produce the highest weight flow, tip speed, and pressure ratio for given design limitations and to determine the manner in which weight flow, tip speed, and pressure ratio are affected by other design variables.

When the position of the symmetrical diagram was properly chosen, the wheel-plus-vortex velocity diagram gave tip speeds, weight flows, and pressure ratios higher than did the symmetrical velocity diagram at all radii, for given aerodynamic design limitations. Both velocity diagrams had constant energy addition per pound of fluid from hub to tip.

For given limiting conditions, the average stage total-pressure ratio is only slightly affected by a deviation of axial velocity from optimum but is considerably reduced by a deviation of relative inlet-air angle from optimum.

The investigation indicates that, if an adiabatic efficiency of 85 percent is assumed, average stage total-pressure ratios of the order of 1.30 and an equivalent weight flow of 26 pounds per second per square foot of frontal area are obtainable for practical design limitations. Present-day production compressors have average stage total-pressure ratios of the order of 1.15 and weight flows of 26 pounds per second per square foot of frontal area.



## INTRODUCTION

In order to obtain added power and increased fuel economy, even for current turbine-temperature limits, the over-all total-pressure ratio of the compressor for both the turbine-propeller and the turbojet engines must be increased. The present method of obtaining high over-all pressure ratios is by the addition of more low pressure-ratio stages. This procedure is undesirable for high-speed aircraft because of the increase in size, weight, and cost of the engine. A more feasible way to obtain a high over-all pressure-ratio compressor is to use higher stage total-pressure ratios. If these higher stage pressure ratios can be obtained without great sacrifice in efficiency and weight flow, more compact high-pressure-ratio multistage compressors can be built.

This analysis was made at the NACA Lewis laboratory to determine how close existing commercial designs are to the practical limit of stage total-pressure ratio. The stagewise variation of axial velocity and relative inlet-air angle through the compressor that produces the highest stage total-pressure ratio for given design limits and design procedure was also determined.

The stage total-pressure ratio of an axial-flow-compressor design is limited by factors such as allowable Mach number, blade loading, and stage static-pressure rise in order to obtain acceptable efficiencies. In this analysis, these factors were considered as restrictions on the design of an inlet stage, a typical intermediate stage, and a typical final stage of a multistage compressor. The quantitative values of most of the limiting factors in use today are not completely known. As more quantitative information becomes available, more will be known of the maximum stage total-pressure ratios that can be used while maintaining acceptable efficiencies and weight flows. Because quantitative knowledge is limited, the qualitative nature of limiting factors and trends are investigated herein. The stagewise design-point characteristics of a multistage compressor were estimated for the optimum stagewise variation of relative inlet-air angle and axial velocity for any given design limits. This optimum is therefore based on existing knowledge and should not be construed to be the absolute optimum.

High tip speed is required to obtain high stage pressure ratios. Because the inlet stage sets the compressor tip speed and weight flow, the inlet stage was designed to obtain a high tip speed with an acceptable weight flow under the design limits imposed. The analysis of the

inlet stage was made for two types of velocity diagram, and from this analysis the inlet stage was selected that would allow the best compromise among the design limits, tip speed, and weight flow. Analyses, based on this inlet-stage, were made of an intermediate stage and a final stage.

From the analyses of the three typical stages, the relative rotor inlet-air angle and axial velocity giving the highest over-all total-pressure ratio were determined. In addition, estimates of stagewise design-point characteristics for several stagewise variations of inlet-air angle and axial velocity other than optimum were made in order to determine the effect on attainable over-all total-pressure ratio. The effect of changing the values of various design limits of the intermediate and final stages on the stagewise design-point characteristics was determined.



## DESIGN PROCEDURE

### Discussion of Design Limits

The maximum allowable Mach number that will permit acceptable efficiency depends on the amount of flow turning through the blade row and, according to available cascade data, to some extent on solidity and relative inlet-air angle. The effects of solidity and relative inlet-air angle on the limiting Mach number are neglected in this investigation. Large turning angles require high-camber blades, which have lower critical Mach numbers than low-camber blades. The maximum allowable Mach number used in this investigation was therefore not a set value but varied with the required turning angle. The relation between maximum allowable Mach number and turning angle used in this analysis was obtained from Bogdonoff's unpublished cascade data. The cascade data used cover only 65-series blower blades in a configuration having a solidity of about 1.5 and a relative inlet-air angle of about $60^{\circ}$. The development of blade sections specifically designed for higher limiting Mach numbers will alter these results appreciably. The maximum allowable Mach number is taken as the average of the critical Mach number and the force-break Mach number, all considered at the design angle of attack of the blades. The critical Mach number is that inlet Mach number at which sonic velocity is reached at some point on the blade. The force-break Mach number is that inlet Mach number above which a large decrease in turning angle and an increase in drag occur. This design angle of attack is selected to obtain the flattest pressure distribution over the suction surface of the blades at a low Mach number. The maximum allowable Mach number for the required turning will hereinafter be designated the limiting Mach number.

Several limits other than the limiting Mach number are used. These limits are blade loading and a parameter describing the tendency of the casing boundary layer to build up and disrupt the flow.

Both rotor turning angle and $\sigma C_L$ (all symbols are defined in appendix A) are a measure of the blade loading and either can be used as

design limit. The values of the limit of $\sigma C_L$ and turning angles used in this investigation were assumed constant with relative inlet air angle. Recent cascade investigations indicate that the maximum obtainable $\sigma C_L$ or turning angle decreases with increasing inlet air angle. Over the range of relative inlet air angles covered in this investigation the effect is small, as indicated in reference 1, and the magnitude of the maximum $\sigma C_L$ for the usual range of solidities is higher than the limiting values used in this investigation. The values of limiting $\sigma C_L$ and turning angle used herein, therefore, are conservative, and for simplicity constant values were used. Both have been widely used as design criteria in axial-flow compressors and curves for both are presented. For a given relative inlet-air angle and for constant axial velocity across the blade row, $\sigma C_L$ and turning angle are functions of each other. In most blade designs, however, some change in axial velocity across the blade row occurs which affects the maximum allowable $\sigma C_L$ value. For any blade configuration, a static-pressure gradient exists from the lowest static pressure on the suction surface to the static pressure behind the blade. For given inlet conditions and work input, the static pressure behind the blade determines the magnitude of the pressure gradient and thus the tendency for flow separation from the suction surface to occur. The static-pressure gradient will be steeper in the case of decreasing axial velocity and flatter in the case of increasing axial velocity than for the case of constant axial velocity across the blade row. The maximum allowable $\sigma C_L$ is therefore lower for decreasing axial velocity and higher for increasing axial velocity, as compared with the case of constant axial velocity. Although the magnitude of the actual turning angle is not affected by changes in axial velocity across the blade row, the same variation of static-pressure rise occurs with changes in axial velocity as previously discussed. Hence, with a decreasing axial velocity the maximum allowable turning is decreased, and for an increasing axial velocity it is increased. In an effort to correct the turning angle for changes in axial velocity, turning angles based on the average of the inlet and outlet axial velocities have been widely used. For a constant corrected turning angle, a decreasing axial velocity results in a smaller actual turning angle and an increasing axial velocity, in a larger actual turning angle. Similarly, the maximum allowable $\sigma C_L$ is a function of relative inlet-air angle; that is, for a given turning angle and constant axial velocity across the blade row, a large relative inlet-air angle will produce a higher static-pressure rise than would be obtained with a low relative inlet-air angle. This relation is shown in figure 1. For constant axial velocity across the blade row and a given relative inlet-air angle, the static-pressure rise is a function of $Y$, the ratio of the change in tangential velocity to rotor tip speed. For a given turning angle, a large relative inlet-air angle produces a larger value of $Y$ and hence a higher pressure rise than does a small relative inlet-air angle. For a given turning angle, the maximum allowable $\sigma C_L$ is a function of both relative inlet-air angle and change in axial velocity across the blade row.

For a given turning angle or $\sigma C_L$, the energy addition per unit mass $YZU_t^2$ increases with increasing relative inlet-air angle. The static-pressure rise across the rotor is therefore increased also. This static-pressure rise is an adverse pressure gradient and promotes the separation of boundary layer along the passage walls. A limiting static-pressure rise parameter should be used so that the build-up of boundary layer along the passage walls will not be excessive and result in separation and disrupted flow. The parameter used to describe this condition is the static-pressure rise divided by the axial dynamic pressure, $\Delta P_s/q_{1,ax}$ and is applied across the blade row at the outer casing. Many factors, such as blade-tip clearance, passage length, temperature, and blade loading, affect the rate at which the boundary layer thickens, and a parameter that would describe the process completely would be very complex. In the absence of a more exact parameter, $\Delta P_s/q_{1,ax}$ was used as a limit in this analysis. Because the static-pressure rise is greatest and the axial velocity least at the outer casing for the velocity diagram considered, the numerical value of the boundary-layer parameter is greater at the tip than at any other radius; hence the application point of this parameter was the outer casing. Unpublished data from a number of single-stage compressors using the types of velocity diagram used in this investigation indicate that the flow breaks down first at the rotor tip radius. The numerical values of the boundary-layer parameter used in this analysis should not be considered as the maximum obtainable. The trend of variation of stage pressure ratio with change in relative inlet-air angle and axial velocity for a given value of $\Delta P_s/q_{1,ax}$ was determined.

In the later stages of a multistage compressor, the static-pressure rise is more critical because the blades have smaller chords than in the first stages, the blades are working against a higher static-pressure gradient, and the boundary layer takes up a greater part of the smaller passage. Conservative values of this boundary-layer parameter have therefore been used. Although the values used have been exceeded in a number of single-stage compressors, good efficiencies have been maintained.

The variation of possible stage pressure ratio for a given set of design limits with a variation of rotor-tip relative inlet-air angle and axial velocity was determined. This analysis was made by calculating the total-pressure ratio for a constant value of each limit involved, that is, $\Delta P_s/q_{1,ax}$, $\sigma C_L$, turning angle, $\Delta\beta'_{c,t}$, and limiting Mach number for various tip axial velocities and relative inlet-air angles. The Mach number at the stator-hub inlet was determined for each of the conditions mentioned to insure that the limiting Mach number had not been exceeded.

## Basic Assumptions and Equations

The analysis was based on the following assumptions:

(1) Isentropic stage process

(2) Constant total enthalpy (constant total temperature) from hub to tip at each axial station

(3) Simple radial equilibrium with no radial flow at each axial station

(4) No change in axial velocity through a blade row at the mean radius

(5) Constant tip diameter through compressor

The three basic equations used in the analysis are

The continuity equation:

$$\int_{r_{1,h}}^{r_{1,t}} 2\pi\rho_1 g V_{1,l}\, r_1\, dr_1 = \int_{r_{2,h}}^{r_{2,t}} 2\pi\rho_2 g V_{2,l}\, r_2\, dr_2$$

The energy equation considered along a streamline:

$$\frac{\gamma}{\gamma-1}\frac{P_{1,s}}{\rho_{1,s}} + \frac{V_1^2}{2} = \frac{\gamma}{\gamma-1}\frac{P_{2,s}}{\rho_{2,s}} + \frac{V_2^2}{2} - U\,\Delta V_\theta$$

The equation for radial equilibrium:

$$\frac{1}{\rho}\frac{dP}{dr} = \frac{V_\theta^2}{r} - V_l\frac{\partial V_r}{\partial l} - V_r\left(\frac{dV_r}{dr}\right)$$

which for no radial flow reduces to

$$\frac{1}{\rho}\frac{dP}{dr} = \frac{V_\theta^2}{r}$$

Constant total enthalpy from hub to tip, resulting from the addition of a vortex by the rotor, and simple radial equilibrium were assumed; and the variation of axial velocity from hub to tip was determined from the energy and equilibrium equations. The assumption of simple radial equilibrium and no radial flow is conservative, inasmuch as higher Mach numbers at the stator hub and higher static-pressure rise across the rotor tip are obtained than would have been if some radial flow, which is present in most compressors, had been assumed.



In the analysis the axial velocity was assumed constant across each blade row at the mean radius. The effects of changes in axial velocity across the blade row are presented for purposes of evaluation.

All pressure ratios for the stagewise design-point characteristics are based on an adiabatic efficiency of 0.85. The over-all total-pressure ratio entering the typical intermediate stage was assumed to be 3.0 and the total-pressure ratio for the typical final stage was assumed as 9.0. For convenience, the corresponding temperature rise at the stage entrances was computed on the assumption of an adiabatic efficiency of 0.85, which implied a slightly higher polytropic efficiency in the final stage than in the intermediate stage.

The inlet, intermediate, and final stages were first calculated on an isentropic basis. From these three stages, the stagewise distribution of stage pressure ratio was determined and then corrected for an adiabatic efficiency of 0.85. These corrected stage pressure ratios were used in the multistage calculations. The assumption of isentropic stage compression and the use of adiabatic efficiencies in the over-all calculations are equal to the assumption that all losses occur between the stages rather than within the stage.

Details of equations used and methods of calculation are given in appendix B.

## Inlet Stage

Because the inlet stage determines the weight flow and the tip speed for the entire compressor, these factors must be kept as high as possible at the inlet stage even if the stage pressure ratio is less than could be obtained if they were reduced. In general, the compromise among weight flow, tip speed, and pressure ratio will vary according to the engine application. The tip speed must be high in a high stage pressure ratio compressor because the energy imparted by the rotor to a unit mass of fluid is the product of the change in tangential velocity component and the speed of the rotor. Because high tip speed is essential to high-stage pressure ratios throughout the compressor, weight flow will not be as high as would be possible with lower tip speeds.

The weight flow obtainable with high tip speeds, however, compares favorably with present low-pressure-ratio compressors. Because the inlet stage is important, the following two types of velocity diagram for this stage were investigated:

(1) A symmetrical velocity diagram at all radii with constant total enthalpy per pound of fluid from hub to tip

(2) A wheel-plus-vortex diagram in which the tangential velocity component entering the rotor is solid-body or wheel type and the change in tangential component through the rotor is a vortex. The stator removes the vortex added by the rotor. This velocity diagram can be symmetrical at one radius only, which may be arbitrarily selected.



Both velocity diagrams have constant energy addition from hub to tip to avoid mixing losses and have increasing axial velocity from tip to hub to satisfy simple radial equilibrium.

Free-vortex-type flow was rejected (reference 1) because it produces low weight flow and low pressure ratio.

Velocity vector diagram nomenclature is illustrated by the typical velocity diagram shown in figure 1.

The second parameter investigated was the rotor-tip relative inlet-air angle $\beta'_{1,t}$. For a given relative Mach number limitation and a symmetrical velocity diagram at some given radius, low relative inlet-air angles produce high weight flows but low tip speeds, whereas high relative inlet-air angles produce the opposite effect. Since both high weight flow and high tip speed are advantageous in the inlet stage, a compromise, which will be discussed later, is necessary.

The third parameter is the ratio of the change in tangential velocity component through the rotor to rotor-tip speed, designated Y. This parameter, as mentioned before, bears directly on the obtainable stage pressure ratio.

The hub-to-tip radius ratio is another parameter. A hub-to-tip radius ratio of 0.5 at the rotor inlet was selected on the basis of reference 2 as a satisfactory compromise among weight flow, tip speed, and pressure ratio.

The principal limit in the inlet stage is the flow Mach number relative to the rotor or stator blades, for high tip speeds and high weight flows per unit frontal area result in high Mach numbers. The limiting Mach number may occur at either the rotor tip or hub, or the stator hub, depending on the type of velocity diagram. Figure 2(a)

shows that for both the wheel-plus-vortex velocity diagram with the symmetrical velocity diagram at the mean radius and the symmetrical velocity diagram at all radii the highest Mach number occurs at the stator hub. Because the stator flow turning is also highest at the hub, the stator-hub Mach number is the limiting factor in the inlet stage. A plot of maximum relative Mach number at the rotor inlet against stator-hub Mach number for constant $Y_m$ values, a hub-tip ratio of 0.5, and rotor-tip relative inlet-air angle of $55^\circ$ is shown in figure 2(a). The maximum relative rotor Mach number occurs at the tip for the wheel-plus-vortex diagram and at the hub for the symmetrical diagram at all radii. The curves crossing the lines of constant $Y_m$ in this figure are curves of limiting Mach number obtained from Bogdonoff's unpublished cascade data previously mentioned. Calculations were made for rotor-tip relative inlet-air angles of $50^\circ$, $55^\circ$, and $60^\circ$. The results shown in figure 2(a) are typical for all three angles.



Only maximum relative Mach numbers at the rotor inlet corresponding to those portions of the curves of constant $Y_m$ (fig. 2(a)) up to the intersection with the curves of limiting Mach number can be used with the blade configuration from which the cascade data were obtained. This configuration consisted of 65-series blower blades having 6-percent thickness and a solidity of 1.5. Other blades and solidity configurations may have higher limiting Mach numbers, permitting higher rotor-tip and stator-hub Mach numbers. Figures 2(b), 2(c), and 2(d) show corresponding curves of specific equivalent weight flow, equivalent tip speed, and stage total-pressure ratio against maximum relative Mach number at the rotor entrance. Figure 2 shows where the limiting Mach number occurs and compares the wheel-plus-vortex diagram and symmetrical diagram at all radii.

The effect of rotor-tip relative inlet-air angle on specific equivalent weight flow, equivalent tip speed, and stage total-pressure ratio as determined for the limiting Mach-number condition at the stator hub for the two types of velocity diagram is shown in figure 3.

These curves are plotted for a $Y_m$ value of 0.25. Figure 3 is obtained from figure 2 and similar curves for the other two angles. The symmetrical diagram at all radii produces slightly higher tip speed and pressure ratio at low relative inlet-air angles and slightly higher specific weight flow at high inlet-air angles.

## Effect of Radial Position of Symmetrical Velocity Diagram for Wheel-plus-Vortex Design

The inlet-stage analysis has thus far considered the position of the symmetrical diagram only at the mean radius for the wheel-plus-vortex diagram. The results of an investigation of the variation of

stator-hub Mach number, specific equivalent weight flow, equivalent tip speed, and stage total-pressure ratio with the radius ratio at which the symmetrical velocity diagram is maintained is shown in figure 4. The rotor-tip Mach number is 0.80 and the relative inlet-air angle is $60^{\circ}$. The curve of limiting Mach number at the stator hub is shown. With the symmetrical diagram at a radius ratio of 0.75 (the mean radius), the stator-hub Mach number is well above the limiting Mach number if the rotor-tip Mach number is 0.80. Moving the position of the symmetrical diagram toward the hub decreases the stator-hub Mach number while the rotor-tip Mach number remains at 0.80; hence high rotor-tip speed is maintained. The shift in radial position of the symmetrical diagram allows the stage pressure ratio, weight flow, and tip speed to be raised without exceeding the limiting Mach number at the stator hub. The effect of shifting the radial position of the symmetrical diagram on specific equivalent weight flow, tip speed, and pressure ratio for $Y_m$ of 0.25 over a range of relative inlet-air angles is shown in figure 5. The solid curve indicates the original position of the symmetrical diagram at a radius ratio of 0.75, as in figure 3. Figures 3 and 5 show that the wheel-plus-vortex diagram produces higher weight flow, pressure ratio, and tip speed than the symmetrical diagram at all radii when the position of the symmetrical diagram is moved from the mean radius toward the hub. In order to obtain high tip speed and a desirable weight flow, a $Y_m$ value of 0.2 was used, which produced a lower pressure ratio than could have been obtained with higher values of $Y_m$ (fig. 4). A $Y_m$ value of 0.15 or 0.10 might be used to gain more tip speed and weight flow at the further expense of pressure ratio. Exceeding the limiting Mach number in the inlet stage would result in lower efficiency but would permit higher tip speed and weight flow. The compromise depends on the application of the engine or the requirements of the turbine and combustion section of the engine. The inlet stage selected for this investigation had an equivalent tip speed of 1120 feet per second, a rotor-tip relative inlet-air angle of $60^{\circ}$, a stage total-pressure ratio of 1.227, and a specific equivalent weight flow of 26.25 pounds per second per square foot of frontal area (35.00 lb/(sec)(sq ft) of annular area). The position of the symmetrical diagram is at a radius ratio of 0.66. These values are shown in figure 4 at the intersections of the $Y_m = 0.20$ and limiting Mach-number curves. The equations used in the inlet-stage analysis are presented in appendix B.

Although the analysis deals primarily with flow having no change in axial velocity across the blade row at the mean radius, table I shows the effect of change in axial velocity through the rotor. This table compares specific equivalent weight flow $W\sqrt{\theta}/A\delta$, equivalent tip speed $U_t/\sqrt{\theta}$, and stage total-pressure ratio $P_2/P_1$ for a 10-percent decrease in axial velocity, no change in axial velocity, and a 10-percent increase in axial velocity, all at the mean radius.

For both types of diagram and for constant $Y_m$, a 10-percent decrease in axial velocity across the rotor permits slight increases in relative Mach number entering the rotor at the tip, specific equivalent weight flow, equivalent tip speed, and stage total-pressure ratio as compared with conditions for no change in axial velocity (table I). A slight decrease in stator-hub Mach number is obtained. For an increase in axial velocity a slight increase in Mach number is obtained. The changes are significant, although small, because specific weight flow, tip speed, and pressure ratio can be raised simultaneously by permitting a decrease in axial velocity through the rotor at the mean radius. Decreases in axial velocity, however, might result in increased boundary-layer thickness and decreased stage efficiency.



## Intermediate Stage

The inlet stage determines the tip speed and the weight flow for the other stages and hence these quantities are not variables in the later stages. The relative inlet-air angle, axial velocity, hub-tip ratio, and radial position of the symmetrical diagram may still be varied. On the basis of the inlet-stage analysis, the wheel-plus-vortex velocity diagram was used in the later stages. The symmetrical velocity diagram was placed at the mean passage radius in the later stages because limiting rotor-tip relative Mach number and stator-hub Mach number are of the same order of magnitude and placing the symmetrical diagram at the mean radius does not decrease one Mach number at the expense of increasing the other.

In the intermediate and final stages, as high a stage pressure ratio as possible should be produced, consistent with any design limitations imposed.

The typical intermediate stage was selected at the point in the compressor where the over-all total-pressure ratio is 3.0. The limiting factors, $\sigma C_L$ at rotor hub, $\Delta P_s/q_{1,ax}$ at the outer casing, limiting Mach number at the rotor tip, and flow turning angle at the rotor tip have been previously discussed.

Possible stage total-pressure ratios and stator-hub limiting Mach numbers against dimensionless axial velocity at the rotor tip $h_{1,t}$ for the various limiting factors and at a rotor-tip relative inlet-air angle of $55^\circ$ are shown in figure 6(a). The same quantities are shown for a relative inlet-air angle of $60^\circ$ in figure 6(b). The possible stage pressure ratio may be limited by one or more of the several limiting factors as shown in figure 6. The rotor-tip relative inlet-air angle and the dimensionless axial velocity at the rotor tip determine which of the factors will be the limit. In general, for constant

relative inlet-air angle at high dimensionless axial velocities, either the rotor tip Mach number or the boundary-layer parameter $\Delta P_s/q_{1,ax}$ or both are the limiting factor, and at low dimensionless axial velocities, turning angle or $\sigma C_L$ is the limiting factor. As the relative inlet-air angle increases, the limiting values of the boundary-layer parameter move to lower pressure ratios and the rotor-tip limiting Mach number moves to lower dimensionless axial velocities. The variation of stage total-pressure ratio and stator-hub Mach number with relative inlet-air angle for various combinations of the limiting factors is shown in figure 7.



Values of the limits used in the intermediate- and final-stage analyses have been exceeded in several single-stage compressors of various configurations, including a high-pressure-ratio configuration that had a pressure ratio of 1.515 and an adiabatic efficiency of 0.89. The limit values are considered reasonable and practical. Curves of possible stage pressure ratio based on the cascade data of reference 3 are presented in figure 7(a) to show further correlation of possible stage pressure ratio with the results of this investigation. The limiting Mach number at the stator hub is shown in figure 7(b) by the nearly horizontal solid curve. This Mach number places a further restriction on the value of the limits that can be used; for example, a value of turning angle $\Delta\beta'_{c,t}$ of $28^\circ$ cannot be used without exceeding the limiting stator-hub Mach number. At high relative inlet-air angles the possible pressure ratio is limited by the boundary-layer parameter and at relative inlet-air angles below about $50^\circ$, by the stator-hub Mach number. The highest pressure ratios are obtained at relative inlet-air angles around $55^\circ$, the value depending on the given value of the limits.

The variation of rotor-tip dimensionless axial velocity with relative inlet-air angle corresponding to the turning angle and $\Delta P_s/q_{1,ax}$ limits used in figure 7 is shown in figure 8. Figure 8 is obtained from curves similar to figure 6 for various relative inlet-air angles and is used to show the range of values of dimensionless axial velocity covered by the limits.

The variation of possible stage total-pressure ratio with relative inlet-air angle for various limits and an axial velocity that would produce a limiting Mach number at the rotor tip is shown in figure 7(a). The axial velocity may be reduced by increasing the passage height, which will cause some reduction in possible pressure ratio. Figure 9 shows the variation of possible stage total-pressure ratios with relative inlet-air angle for two dimensionless axial velocities less than those required for limiting rotor-tip Mach numbers at the rotor tip, and a given set of limits. These curves are an envelope of the various limit curves and are obtained from cross plots of curves similar to figure 6. The curves show that for a given dimensionless axial velocity

only a small range of relative inlet-air angle will produce the highest pressure ratio for a given set of limits and that a deviation from this range will greatly reduce the possible pressure ratio. A change in dimensionless axial velocity does not have a great effect on the optimum relative inlet-air angle. For a given dimensionless axial velocity, the turning angle is the limiting factor at low relative inlet-air angles. As the relative inlet-air angle is increased, $\sigma C_L$ may become the limiting factor until the boundary-layer parameter curve is reached. The boundary-layer parameter then becomes the limiting factor until the relative rotor-tip Mach number is reached.



The relative magnitude of the boundary-layer parameter $\Delta P_s/q_{2,ax}$ at the stator hub and tip compared with the rotor tip, and the effect of changes in turning-angle limit and $\Delta P_s/q_{1,ax}$ at the rotor tip on $\Delta P_s/q_{2,ax}$ at the stator tip and hub are shown in table II. The table covers a range of $\Delta P_s/q_{1,ax}$ and $\Delta\beta'_{c,t}$ values at the rotor tip so that a correlation can be made.

All stator values are lower than rotor tip values. Table II shows also that $\Delta P_s/q_{2,ax}$ at the stator hub and tip is more affected by $\Delta\beta'_{c,t}$ changes than by $\Delta P_s/q_{1,ax}$ across the rotor at the outer case. The general discussion of $\Delta P_s/q_{1,ax}$ at the rotor tip dealt with this relation.

## Final Stage

An investigation similar to that for the intermediate stage was carried out for a typical final stage. The over-all total-pressure ratio at the inlet to this stage was assumed to be 9.0. The results of the analysis are presented in figures 10 to 13. The equations used to calculate the results are given in appendix B.

The corresponding figures for the intermediate and final stages are quite similar except for the numerical values. The possible total-pressure ratios for a given set of limits are lower for the final stage than for the intermediate stage because of the lower equivalent tip speed in the later stages due to higher temperature. The dimensionless axial velocities required to produce a limiting Mach number at the rotor tip are higher in the final stages because of the higher velocity of sound. The optimum relative inlet-air angle for a given set of limits is slightly higher in the final stage than that for the intermediate stage and a deviation from the optimum relative inlet-air angle for a given dimensionless axial velocity and set of limits produces a smaller decrease in total-pressure ratio in the final stage than in the intermediate stage (see figs. 9 and 13).

## MULTISTAGE ANALYSIS

By use of the results of the three stage analyses, an estimate of the over-all total-pressure ratio of a multistage compressor can be made. In order to obtain the highest total-pressure ratio for a given set of limits, that is, specified values of $\Delta P_s/q_{1,ax}$, $(\sigma C_L)_h$, $\Delta\beta'_{c,t}$, and Mach number, a definite relative inlet-air angle and dimensionless axial velocity are obtained as shown in figures 7, 8, 11, and 12. Generally the specified values of $\sigma C_L$, $\Delta\beta'_{c,t}$, and $\Delta P_s/q_{1,ax}$ cannot all be satisfied at the same time. The two quantities permitting the highest pressure ratio without exceeding the specified value of the third parameter are used. These optimum values of rotor-tip dimensionless axial velocity, relative inlet-air angle, and stage total-pressure ratio for the intermediate and final stages are plotted with the values at the inlet stage against over-all total-pressure ratio on semilog coordinates. Smooth curves were faired through the data. Figure 14 presents a typical curve for $\Delta\beta'_{c,t} = 20^\circ$, $(\sigma C_L)_h = 1.1$, and $\Delta P_s/q_{1,ax} = 1.6$. The boundary-layer parameter is the most severe limitation on stage pressure ratio at high relative inlet-air angles, and the later stages require lower relative inlet-air angles than the inlet stage does to produce the maximum total-pressure ratio for a specified set of conditions. Pressure ratio was compromised at the inlet stage to obtain high tip speed and satisfactory weight flow. Stage pressure ratio rose from the inlet value to a maximum in the intermediate stages, after which the increasing severity of the boundary-layer parameter and blade-loading parameters limited the stage pressure ratios to lower values in the final stages. The increase in dimensionless axial velocity at the rotor tip through the compressor has the advantage of tending to keep the boundary layer thin, but has the disadvantage of making the diffuser design more difficult. These results were obtained for optimum conditions, that is, they were the best results for a specified set of limits. This optimum does not indicate an absolute maximum value. The curves obtained from the three stage analyses permit a stage-by-stage calculation of stagewise design-point characteristics. The results are shown in figure 15. Figure 15 shows the variation of over-all total-pressure ratio, stage total-pressure ratio, rotor-tip relative inlet-air angle, rotor-tip axial Mach number based on total temperature, and dimensionless axial velocity at the rotor tip with the number of stages in the compressor for five conditions. The limits used in the figure are $\Delta\beta'_{c,t} = 20^\circ$, $\Delta P_s/q_{1,ax} = 1.6$, limiting Mach number at rotor tip, and $(\sigma C_L)_h = 1.1$. The pressure ratios and axial Mach number are based on an adiabatic efficiency of 0.85.

Curve A represents the optimum analysis conditions for this set of limits; that is, the stagewise variation of inlet-air angle, which should be lower in the final stages than in the inlet stage, and of axial

velocity, which should increase stagewise, that produces the highest over-all total-pressure ratio.

Curves B, C, and E were obtained from cross plots similar to figures 9 and 13 of stage total-pressure ratio against relative inlet-air angle for various dimensionless axial velocities at the rotor tip and a given set of limits.



The effect of deviation from the optimum stagewise variation of relative inlet-air angle and axial velocity is shown by the four curves, B to E. The results of a constant relative inlet-air angle and an axial velocity that will give the Mach-number limit at the rotor tip are shown by curve D. These conditions produce low pressure ratios as compared with curve A. The stagewise characteristics for constant relative inlet-air angle and constant axial Mach number, shown by curve E, are of lower values than for curve D. Curves D and E show that possible over-all total-pressure ratio is sensitive to deviations of relative inlet-air angle at the rotor tip other than the optimum stagewise distribution. The conditions represented by curve D give the axial-velocity distribution that is optimum for the specified relative inlet-air angle because this axial velocity results in the limiting Mach number at the rotor tip. Curve E shows the effect of deviation from the optimum stagewise distribution of both relative inlet-air angle and axial velocity. The stagewise characteristics of a compressor having constant axial Mach number throughout are shown by curve C. The over-all total-pressure ratio for curve C is significantly higher than for curves D and E, although it remains less than that of curve A. Curve B shows the characteristics for constant axial-velocity ratio downstream of the point where the over-all total-pressure ratio is 3.0. This curve most closely approaches the optimum conditions, and may be even more advantageous than the optimum conditions because the axial velocity is much lower at the compressor outlet. Such a compressor would require only one more stage than the optimum compressor to produce the same over-all pressure ratio. Figure 15 shows that the stagewise characteristics are rather poor for designs having constant relative inlet-air angle (curves D and E) compared with designs which use the optimum relative inlet-air angle for the specified axial velocity (curves B and C).

Only a small range of relative inlet-air angle for a given axial velocity produces the highest pressure ratio and a deviation from this range of relative inlet-air angle results in a large decrease in total-pressure ratio (figs. 9 and 13). Changes in axial velocity from optimum also result in a decrease in possible pressure ratio. However, the decrease in pressure ratio which occurs for a decrease in axial velocity is small compared with the decrease which occurs for a change in relative inlet-air angle.

Although decreasing the axial-velocity distribution from the optimum distribution may be advantageous in obtaining lower compressor-outlet axial velocities and lower outlet hub-to-tip ratios, no advantage is gained by deviating from the optimum relative inlet-air-angle distribution.

As previously mentioned, the outlet axial-velocity ratio of the optimum compressor (curve A) is quite high and produces some problems in diffuser design. For this reason, either constant axial Mach number (curve C) or constant axial-velocity (curve B) designs may be more desirable. Constant axial-velocity design (downstream of the point where the over-all total-pressure ratio is 3.0) produces lower outlet axial velocities than does constant axial Mach-number design and has a higher over-all pressure ratio for a given number of stages.



The effect of changing the limit values on stagewise characteristics of a compressor having constant axial velocity downstream of the point where the over-all total-pressure ratio is 3.0 is shown in figure 16. All curves are based on optimum relative inlet-air angle for the specified limit values.

Increasing the value of $\Delta\beta'_{c,t}$ from 20° to 28° (cases I and III) or increasing the value of $\Delta P_s/q_{1,ax}$ from 1.6 to 2.0 (cases I and IV) has very little separate effect on the over-all pressure ratio. The $\sigma C_L$ limit is reached first and increasing the value of the other limits has no effect in the middle stages and only a slight effect in the final stages. Increasing the limiting $\sigma C_L$ value from 1.0 to 1.2 (cases I and II) produces a marked effect because it permits the stage pressure ratio of the intermediate stages to be raised. Increasing all the limits (cases I and V) produces a significant increase in over-all total-pressure ratio. This increase was sufficient to allow the elimination of one stage yet to maintain the same over-all total-pressure ratio as cases I, III, and IV.

## CONCLUSIONS

The following conclusions were obtained from the analytical investigation of high stage pressure ratio axial-flow multistage compressors:

(1) The wheel-plus-vortex velocity diagram, when the radial position of the symmetrical velocity is properly chosen, results in tip speeds, weight flows, and total-pressure ratios higher than the symmetrical velocity diagram at all radii with constant energy addition from hub to tip when compared on a limiting Mach number basis.

(2) In order to obtain maximum over-all total-pressure ratio with satisfactory weight flow for the limits used, the stage pressure ratio should be low in the inlet stage, should increase in the intermediate stages, and then decrease in the final stages of the compressor.

(3) In order to obtain maximum over-all total-pressure ratio for the limits used, the axial velocity should increase stagewise through the compressor and the relative inlet-air angle at the rotor tip should be lower in the later stages than in the inlet stage.



(4) For a given set of limiting conditions, constant stagewise axial Mach number design and a design having constant stagewise axial velocity downstream of the point in the compressor where the over-all total-pressure ratio is 3.0 produced nearly as high an average stage total-pressure ratio as the optimum design and had appreciably lower outlet axial velocities.

(5) For a given set of limiting conditions, designs having constant relative inlet-air angle produced appreciably lower average stage total-pressure ratios than the designs that used the optimum relative inlet-air angle stagewise distribution. These results were obtained because the dimensionless axial velocity must change if the relative inlet-air angle is changed appreciably in order to maintain limiting conditions.

(6) An increase of the allowable value of the $\sigma C_L$ parameter while the other parameters remained constant had an appreciable effect on pressure ratios. Increasing the allowable values of $\Delta\beta'_{c,t}$ and $\Delta P_s/q_{1,ax}$ parameters while the other parameters are kept constant had little effect on the pressure ratio. Increasing all parameters simultaneously results in a significant increase in over-all pressure ratio.

(7) For an assumed adiabatic efficiency of 85 percent, average stage total-pressure ratios of the order of 1.30 and a weight flow of 26 pounds per second per square foot of frontal area were indicated as being obtainable with the reasonable and practical design limitations used.

Lewis Flight Propulsion Laboratory
National Advisory Committee for Aeronautics
Cleveland, Ohio

# APPENDIX A

## SYMBOLS

The following symbols are used in this report:

| | |
|---|---|
| $A$ | frontal area, based on rotor-tip diameter, sq ft |
| $a$ | local speed of sound, ft/sec |
| $C_L$ | lift coefficient |
| $c_p$ | specific heat at constant pressure, Btu/(lb)(°F) |
| $f$ | function |
| $g$ | standard acceleration due to gravity, 32.174 ft/sec$^2$ |
| $h$ | dimensionless axial velocity, ratio of axial velocity to rotor tip speed |
| $J$ | mechanical equivalent of heat, 778 ft-lb/Btu |
| $M$ | Mach number, $V/a$ |
| $P$ | absolute pressure, lb/sq ft |
| $q$ | dynamic pressure, $\frac{1}{2}\rho V^2$, lb/sq ft |
| $R$ | gas constant, ft-lb/(lb)(°R) |
| $r$ | radius, ft |
| $T$ | absolute temperature, °R |
| $U$ | blade speed, ft/sec |
| $U/\sqrt{\theta}$ | equivalent blade speed corrected to standard NACA sea-level conditions, ft/sec |
| $V$ | absolute velocity, ft/sec |
| $V'$ | relative velocity of fluid with respect to rotor, ft/sec |
| $W$ | weight flow, lb/sec |

$\frac{W\sqrt{\theta}}{\delta A}$ specific equivalent weight flow, weight flow per unit frontal area corrected to standard NACA sea-level conditions, lb/(sec)(sq ft)

X ratio of absolute tangential velocity to rotor-tip speed

Y ratio of change in tangential velocity through rotor to rotor-tip speed

Z ratio of blade speed at any radius to blade speed at tip

$\beta$ angle between absolute velocity vector and rotor axis, deg

$\beta'$ angle between relative inlet-air velocity vector and rotor axis, deg

$\Delta\beta'$ relative turning angle through rotor, deg

$\gamma$ ratio of specific heats $c_p/c_v = 1.3947$

$\delta$ ratio of inlet total pressure to standard NACA sea-level pressure (2116.2 lb/sq ft)

$\theta$ ratio of inlet total temperature to standard NACA sea-level temperature (518.6 $^{\circ}$R)

$\rho$ mass density of air, slugs/cu ft

$\sigma$ blade-element solidity, chord/spacing = $\frac{\text{number of blades} \times \text{chord}}{2\pi r}$

Subscripts:

0 standard conditions

1 upstream of rotor

2 downstream of rotor and upstream of stator

3 downstream of stator

av average

ax axial

c corrected for change in axial velocity through blade row

h hub radius

| | |
|---|---|
| $l$ | axial direction |
| m | mean radius |
| r | any given radius, or radial direction |
| s | static conditions |
| T | total conditions |
| t | tip radius |
| $\theta$ | tangential direction |

Superscript:

| | |
|---|---|
| ' | relative to rotor |

# APPENDIX B

## EQUATIONS USED IN INVESTIGATION

### General Assumptions

The equations are based on the following assumptions:

(1) Constant tip diameter

(2) Constant axial velocity through the blade row at the mean radius

(3) Isentropic stage compression

(4) Constant total enthalpy from hub to tip

(5) Simple radial equilibrium of pressure and no radial flow

### Inlet Stage

Wheel-plus-vortex velocity diagram. - This diagram has solid body rotation through guide vanes with vortex rotation added by the rotor and removed by the stator. The velocity diagram is symmetrical at one radius. Values of $\beta'_{1,t}$ and $Y_m$ are assumed; $Z_{1,h}$ has been assumed to be 0.50. The variation of X, Y, and h can be determined as follows:

$$X_r = \frac{Z_r - Y_r}{2} \tag{B1}$$

where r is the radius at which the symmetrical diagram is maintained.

For solid-body rotation after the inlet guide vanes,

$$X_{1,t} = \frac{X_1}{Z} \tag{B2}$$

Since the rotor adds a vortex to the flow,

$$Y_t = YZ \tag{B3}$$

Assuming constant total enthalpy from hub to tip, an isentropic process, solid-body rotation, and simple radial equilibrium with no radial flow, the energy equation gives

$$h_1^2 = 2X_{1,t}^2 (1 - Z^2) + \frac{(1 - X_{1,t})^2}{\tan^2\beta'_{1,t}} \tag{B4}$$

The tip speed is found by writing the energy equation between the rotor inlet and a stagnation point in the free stream:

$$U_t^2 = \frac{a_0^2}{\frac{h_{1,t}^2 + (1 - X_{1,t})^2}{M'^2_{1,t}} + \frac{\gamma - 1}{2}(X_{1,t}^2 + h_{1,t}^2)} \tag{B5}$$

Values of $M'_{1,t}$ are assumed in equation (B5).

The hub conditions are similarly found to be

$$X_{1,h} = X_{1,t}\, Z_h \quad \text{and} \quad Y_h = \frac{Y_t}{Z_h} \tag{B6}$$

$$M'^2_{1,h} = \frac{h_{1,h}^2 + (Z_h - X_{1,h})^2}{\left(\frac{a_0}{U_t}\right)^2 - \frac{\gamma - 1}{2}(X_{1,h}^2 + h_{1,h}^2)} \tag{B7}$$

The weight flow is given by

$$W = \int_{r_h}^{r_t} \rho g h U_t\, 2\pi r\, dr$$

which in terms of the known quantities becomes

$$W = 2\pi r_t^2\, U_t \rho_0 g \int_{Z_h}^{1.0} \left\{ 1 - \frac{\gamma - 1}{2a_0^2} \left[ h_t^2 + 2X_t^2 (1 - Z^2) + X_t^2 Z^2 \right] U_t^2 \right\}^{\frac{1}{\gamma - 1}} \left[ h_t^2 + 2X_t^2 (1 - Z^2) \right]^{1/2} Z\, dZ \tag{B8}$$

which may be numerically or mechanically integrated.

The stator-hub radius is determined from the continuity equation for the known weight flow and velocity distribution downstream of the rotor.

By use of the energy equation across the rotor and the continuity equation, the weight flow entering the stator is

$$W = 2\pi r_t^2 \rho_0 g U_t \int_{Z_h}^{1.0} \left[ h_{1,m}^2 - 2X_{1,t}^2 (Z^2 - Z_m^2) - 4X_{1,t} Y_t \ln \frac{Z}{Z_m} \right]^{1/2} \left\{ 1 - \frac{\gamma - 1}{2} \left( \frac{U_t}{a_0} \right)^2 \left[ h_{1,m}^2 - 2X_{1,t}^2 (Z - Z_m^2) - 4X_{1,t} Y_t \ln \frac{Z}{Z_m} + (X_1 + Y)^2 - 2Y_t \right] \right\}^{\frac{1}{\gamma - 1}} Z \, dZ \qquad \text{(B9)}$$

Various values of $Z_h$ are assumed and equation (B9) is evaluated until the weight flow equals that known for the rotor. Thus the stator $Z_h$ is found and the channel shape is determined. This procedure can be used for any stage.

The distribution of axial velocity entering the stator can be obtained from the following equation:

$$h_2^2 = h_{1,m}^2 - 2X_{1,t}^2 (Z^2 - Z_m^2) - 4X_{1,t} Y_t \ln \frac{Z}{Z_m} \qquad \text{(B10)}$$

for any radial position.

The stage total-pressure ratio is determined by assuming an isentropic process and writing the energy equation, taking into account the energy added to the flow by the rotor. The resulting equation is

$$\frac{P_{2,T}}{P_{1,T}} = \left[ 1 + (\gamma - 1) Y_t \left( \frac{U_t}{a_0} \right)^2 \right]^{\frac{\gamma}{\gamma - 1}} \qquad \text{(B11)}$$

The stator-hub Mach number is investigated to determine whether the critical Mach number is exceeded. Only the stator hub need be investigated as this point has the highest local Mach number. The following equation is obtained from the energy equation, assuming an isentropic process and a perfect gas:

$$\left(\frac{1}{M_{2,h}}\right)^2 = \frac{(\gamma - 1)\, c_p g J T_{1,T} \left(\frac{P_{2,T}}{P_{1,T}}\right)^{\frac{\gamma - 1}{\gamma}}}{\left[h_{2,h}^2 + (X_h + Y_h)^2\right] U_t^2} - \frac{\gamma - 1}{2} \qquad \text{(B12)}$$



Symmetrical velocity diagram at all radii. - This velocity diagram has wheel-minus-vortex rotation through the guide vanes; the rotor adds a vortex to the flow and the stator removes this vortex.

As in the wheel-plus-vortex velocity diagram, $\beta'_{1,t}$, $Y_m$, and $M'_{1,t}$ are assumed; $Z_{1,h}$ has been assumed to be 0.50.

Since a vortex is added by the rotor,

$$Y = \frac{Y_t}{Z} \qquad \text{(B13)}$$

The equation of the symmetrical diagram is

$$2X_1 + Y = Z \qquad \text{(B14)}$$

or

$$X_1 = \frac{Z}{2} - \frac{Y}{2Z} \qquad \text{(B15)}$$

The distribution of axial velocity entering the rotor is

$$h_1^2 = h_{1,t}^2 - Y_t \ln \frac{1.0}{Z} + \frac{1}{2}(1.0 - Z^2) \qquad \text{(B16)}$$

The axial-velocity distribution entering the stator is

$$h_2^2 = h_{1,m}^2 + \frac{1}{2}(Z_m^2 - Z^2) + Y_t \ln \frac{Z_m}{Z} \qquad \text{(B17)}$$

Equations for $U_t$, weight flow, stage total-pressure ratio, and stator-hub Mach number similar to those for the wheel-plus-vortex diagram may be written:

$$U_t^2 = \frac{a_0^2}{\frac{h_{1,h}^2 + (Y_h + X_{1,h})^2}{M'^2_{1,h}} + \frac{\gamma - 1}{2}\left(h_{1,h}^2 + X_{1,h}^2\right)} \tag{B18}$$



$$W = 2\pi\rho_0 g r_t^2 U_t \int_{Z_h}^{1.0} \left[1 - \frac{\gamma - 1}{2}\left(h_1^2 + X_1^2\right)\left(\frac{U_t}{a_0}\right)^2\right]^{\frac{1}{\gamma - 1}} h_1 Z \, dZ \tag{B19}$$

$$\frac{P_{2,T}}{P_{1,T}} = \left[1 + (\gamma - 1)\, Y_t \left(\frac{U_t}{a_0}\right)^2\right]^{\frac{\gamma}{\gamma - 1}} \tag{B20}$$

$$\left(\frac{1}{M_{2,h}}\right)^2 = \frac{\left(\frac{P_{2,T}}{P_{1,T}}\right)^{\frac{\gamma - 1}{\gamma}}}{\left(\frac{U_t}{a_0}\right)^2 \left[h_{2,h}^2 + (X_h + Y_h)^2\right]} - \frac{\gamma - 1}{2} \tag{B21}$$

## Intermediate and Final Stages

For the intermediate and final stages, the wheel-plus-vortex velocity diagram, which was symmetrical at the mean radius, was used. The weight flow and tip speed are set by the inlet stage and are therefore known. Values of $\beta'_{1,t}$ and $h_{1,t}$ are assumed. The over-all total-pressure ratio at the intermediate stage entrance is assumed to be 3.0; that at the final stage entrance, 9.0.

The turning of the flow at the rotor tip, based on limiting Mach number, is calculated as follows:

$$V'_{1,t} = \frac{h_{1,t}\, U_t}{\cos \beta'_{1,t}} \tag{B22}$$

$$a = \sqrt{\gamma g R T_s}$$

$$M'_{1,t} = \frac{V'_{1,t}}{a_{1,t}} \tag{B23}$$

The value of $\Delta\beta'_{c,t}$ corresponding to $M'_{1,t}$ is selected from a chart based on Bogdonoff's unpublished cascade data. In using this chart, the assumption is made that blade thickness, solidity, and relative inlet-air angle are near 6 percent, 1.5, and 60°, respectively.



To find $Z_{1,h}$

$$W = 2\pi\rho_0 g r_t^2 U_t \int_{Z_h}^{1.0} \left[\frac{T_T}{T_0} - \frac{\gamma - 1}{2}\left(\frac{U_t}{a_0}\right)^2 (h_1^2 + X_1^2)\right]^{\frac{1}{\gamma - 1}} h_1 Z \, dZ \tag{B24}$$

By assuming values of $Z_h$ and evaluating the integral, $Z_{1,h}$ can be found, since the weight flow must equal that for the inlet stage.

The axial-velocity distribution entering the stator is given by

$$h_2^2 = h_{1,m}^2 - 2X_{1,t}^2 (Z^2 - Z_m^2) - 4X_{1,t} Y_t \ln \frac{Z}{Z_m} \tag{B25}$$

The rotor relative inlet-air angle corrected for variation in axial velocity is given by

$$\left.\begin{aligned} \beta'_{1,t,c} &= \tan^{-1}\left(\frac{1 - X_{1,t}}{h_{av,t}}\right) \\ \beta'_{1,t,c} - \Delta\beta'_{c,t} &= \beta'_{2,c,t} \end{aligned}\right\} \tag{B26}$$

The stage total-pressure ratio based on allowable Mach number is

$$\frac{P_{2,T}}{P_{1,T}} = \left[1 + (\gamma - 1)\frac{Y_t}{\frac{T_{1,T}}{T_0}}\left(\frac{U_t}{a_0}\right)^2\right]^{\frac{\gamma}{\gamma - 1}} \tag{B27}$$

The $\Delta P_s/q_{1,ax}$ term is computed from the following equation:



$$\frac{\Delta P_s}{q_{1,ax}} = \left\{\left[1 + \frac{\gamma - 1}{2a_1^2}\left(V'^2_1 - V'^2_2\right)\right]^{\frac{\gamma}{\gamma - 1}} - 1\right\}\frac{2}{\gamma M^2_{ax}} \tag{B28}$$

which is derived from the energy equation and is based on isentropic stage conditions.

Values of $Y_t$ are assumed from which $h_{2,t}$ values are calculated. The $h_{2,t}$ values are used to compute $V'^2_2$ so that a range of $\Delta P_s/q_{1,ax}$ values covers a range of $Y_t$. Values of $Y_t$ are then obtainable for desired values of $\Delta P_s/q_{1,ax}$ and corresponding stage total-pressure ratios can be computed.

For the turning limitation, a range of $Y_t$ values are assumed and $\Delta\beta'_{t,c}$ values are computed by use of the following equations:

$$\Delta\beta'_{c,t} = \beta'_{1,t,c} - \beta'_{2,t,c} = \tan^{-1}\left[\frac{Z_t - X_{1,t}}{h_{av,t}}\right] - \tan^{-1}\left[\frac{(Z - X_1 - Y)_t}{h_{av,t}}\right] \tag{B29}$$

$$h_{av,t} = \frac{h_{2,t} + h_{1,t}}{2} \tag{B30}$$

$$h^2_{2,t} = h^2_{1,t} - 4X_{1,t}\,Y_t \ln\frac{1}{Z_m} \tag{B31}$$

Values of $\Delta\beta'_{c,t}$ are plotted against corresponding values of $Y_t$ and $Y_t$ is determined for selected values of $\Delta\beta'$. These values of $Y_t$ were used to determine stage total-pressure ratio based on $\Delta\beta'_{c,t}$.

Stator-hub Mach numbers for various values of $\Delta P_s/q_{1,ax}$ and $\Delta\beta'_{c,t}$ are determined by use of the $Y_t$ values corresponding to the selected values of $\Delta P_s/q_{ax}$ and $\Delta\beta'_{c,t}$, which are inserted in the following equations:

$$h_{2,h}^2 = h_{1,t}^2 + 2X_{1,t} - 2X_{1,t}^2 Z_h^2 + 4X_{1,t} Y_t \ln \frac{Z_m}{Z_h} \tag{B32}$$

$$\left(\frac{1}{M_{2,h}}\right)^2 = \frac{\left(\frac{a_0}{U_t}\right)^2 \left(\frac{P_{2,T}}{P_{1,T}}\right)^{\frac{\gamma-1}{2}} \frac{T_{1,T}}{T_0}}{h_{2,h}^2 + (X_{1,h} + Y_h)^2} - \frac{\gamma - 1}{2} \tag{B33}$$

The $\sigma C_L$ limitation is calculated by means of the following relation:

$$(\sigma C_L)_h^2 = \frac{4 Y_h^2}{h_{av,h}^2 + (Z_h - X_h)^2 - (Z_h - X_h) Y_h + \frac{Y_h^2}{4}} \tag{B34}$$

The value of $Y_h$ corresponding to the selected value of $(\sigma C_L)_h$ is used to calculate the stage total-pressure ratio since

$$Y_t = Z_h Y_h$$

and $Z_h$ is known and

$$\frac{P_{2,T}}{P_{1,T}} = \left[1 + (\gamma - 1) \frac{Y_t}{\frac{T_{1,T}}{T_0}} \left(\frac{U_t}{a_0}\right)^2\right]^{\frac{\gamma}{\gamma - 1}}$$

## REFERENCES

1. Howell, A. R., and Carter, A. D. S.: Fluid Flow through Cascades of Aerofoils. Rep. No. R. 6, British N.G.T.E., Sept. 1946.

2. Sinnette, John T., Jr.: Analysis of Effect of Basic Design Variables on Subsonic Axial-Flow-Compressor Performance. NACA Rep. 901, 1948. (Formerly NACA RM E7D28.)

3. Wu, Chung-Hua, Sinnette, John T., Jr., and Forrette, Robert E.: Theoretical Effect of Inlet Hub-Tip-Radius Ratio and Design Specific Mass Flow Design Performance on Axial-Flow Compressors. NACA TN 2068, 1950.

TABLE I - EFFECT OF AXIAL-VELOCITY VARIATION ON INLET-STAGE OPERATING CONDITIONS FOR TWO SELECTED $Y_m$ VALUES

Wheel-plus-vortex diagram, symmetrical at mean radius

| Change in $V_{ax}$ through rotor at mean radius | Selected $Y_m$ | $M'_{1,t}$ | $M_{2,h}$ | Specific equivalent weight flow $W\sqrt{\theta}/\delta A$ | Equivalent tip speed $U_t/\sqrt{\theta}$ | Stage total-pressure ratio $P_2/P_1$ |
|---|---|---|---|---|---|---|
| 10-percent decrease | 0.20<br>.30 | 0.755<br>.740 | 0.814<br>.782 | 27.55<br>26.20 | 1057<br>943 | 1.210<br>1.244 |
| No change | 0.20<br>.30 | 0.735<br>.726 | 0.814<br>.784 | 27.10<br>25.85 | 1030<br>925 | 1.19<br>1.234 |
| 10-percent increase | 0.20<br>.30 | 0.720<br>.712 | 0.817<br>.785 | 26.75<br>25.50 | 1010<br>910 | 1.183<br>1.225 |

Symmetrical diagram at all radii

| Change in $V_{ax}$ through rotor at mean radius | $Y_m$ | $M'_{1,h}$ | $M_{2,h}$ | $W\sqrt{\theta}/\delta A$ | $U_t/\sqrt{\theta}$ | $P_2/P_1$ |
|---|---|---|---|---|---|---|
| 10-percent decrease | 0.20<br>.30 | 0.779<br>.730 | 0.810<br>.770 | 28.25<br>27.05 | 1082<br>955 | 1.211<br>1.273 |
| No change | 0.20<br>.30 | 0.742<br>.685 | 0.812<br>.776 | 27.42<br>26.75 | 1027<br>938 | 1.191<br>1.240 |
| 10-percent increase | 0.20<br>.30 | 0.709<br>.683 | 0.816<br>.795 | 26.40<br>25.95 | 990<br>930 | 1.175<br>1.238 |

TABLE II - VARIATION OF BOUNDARY-LAYER PARAMETER $\frac{\Delta P_s}{q_{2,ax}}$ FOR THE STATOR WITH TWO ROTOR CONDITIONS

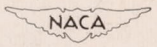


| Rotor tip | | $\Delta P_s/q_{2,ax}$ | | | |
|---|---|---|---|---|---|
| | | Intermediate stage | | Final stage | |
| $\frac{\Delta P_s}{q_{1,ax}}$ | $\Delta\beta'_{c,t}$ (deg) | Hub | Tip | Hub | Tip |
| 1.6 | 20 | 0.839 | 0.052 | 0.896 | 0.029 |
| 1.6 | 28 | 1.076 | 0.132 | 1.342 | 0.040 |
| 2.0 | 20 | 0.844 | 0.077 | 0.981 | 0.023 |
| 2.0 | 28 | 1.251 | 0.149 | 1.491 | 0.055 |

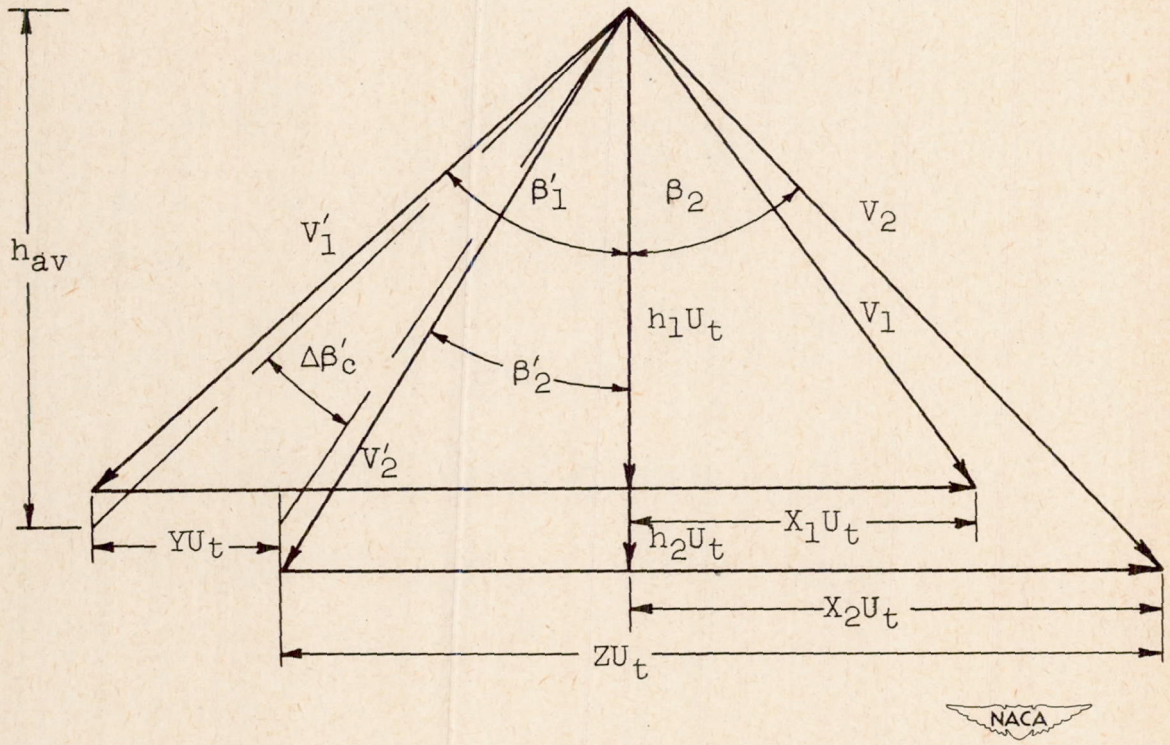


Figure 1. - Typical velocity diagram.

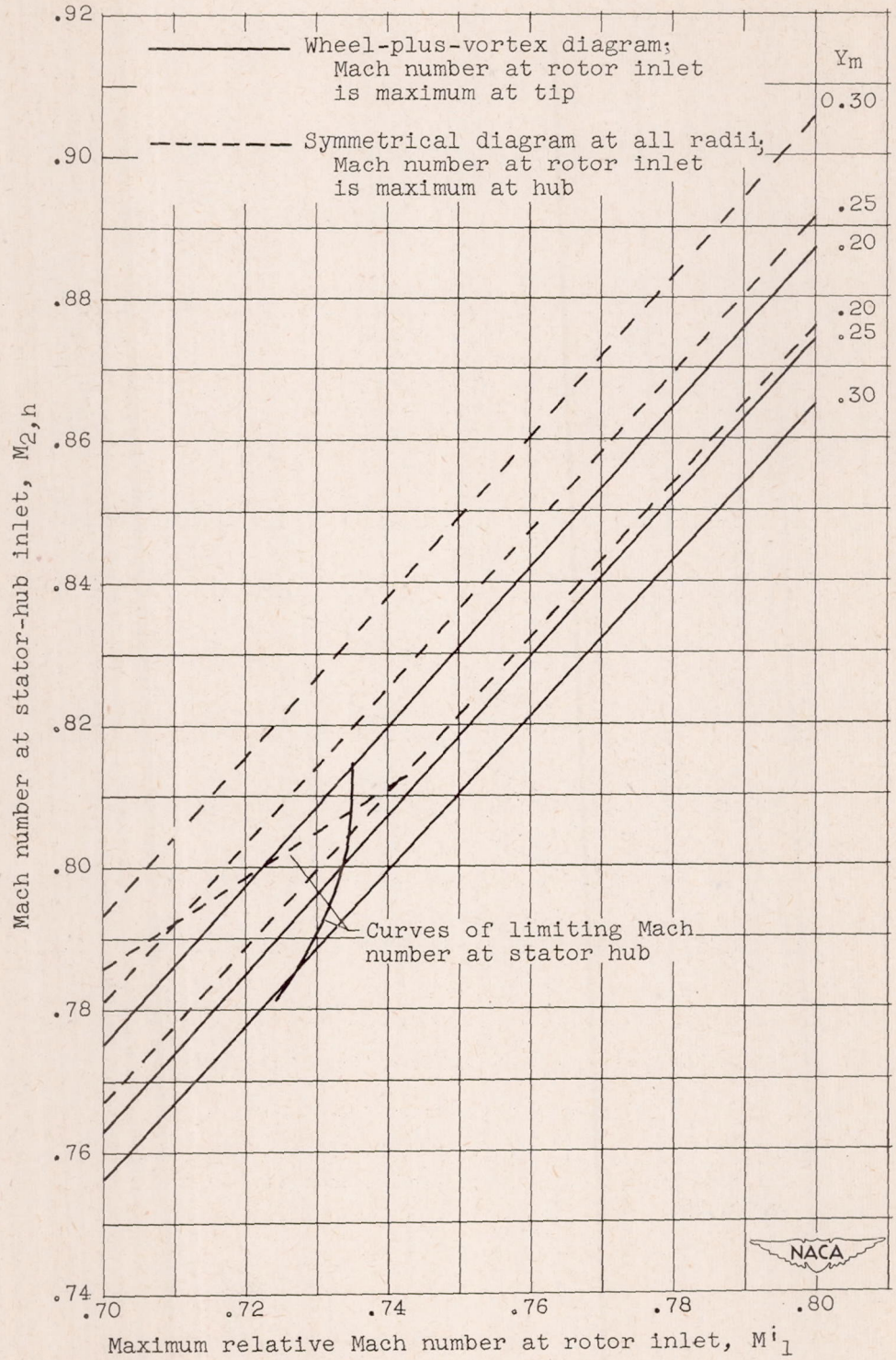


(a) Mach number at stator-hub inlet.

Figure 2. - Operating conditions of inlet stage. Hub-to-tip ratio, 0.5; rotor-tip relative inlet-air angle, 55°.

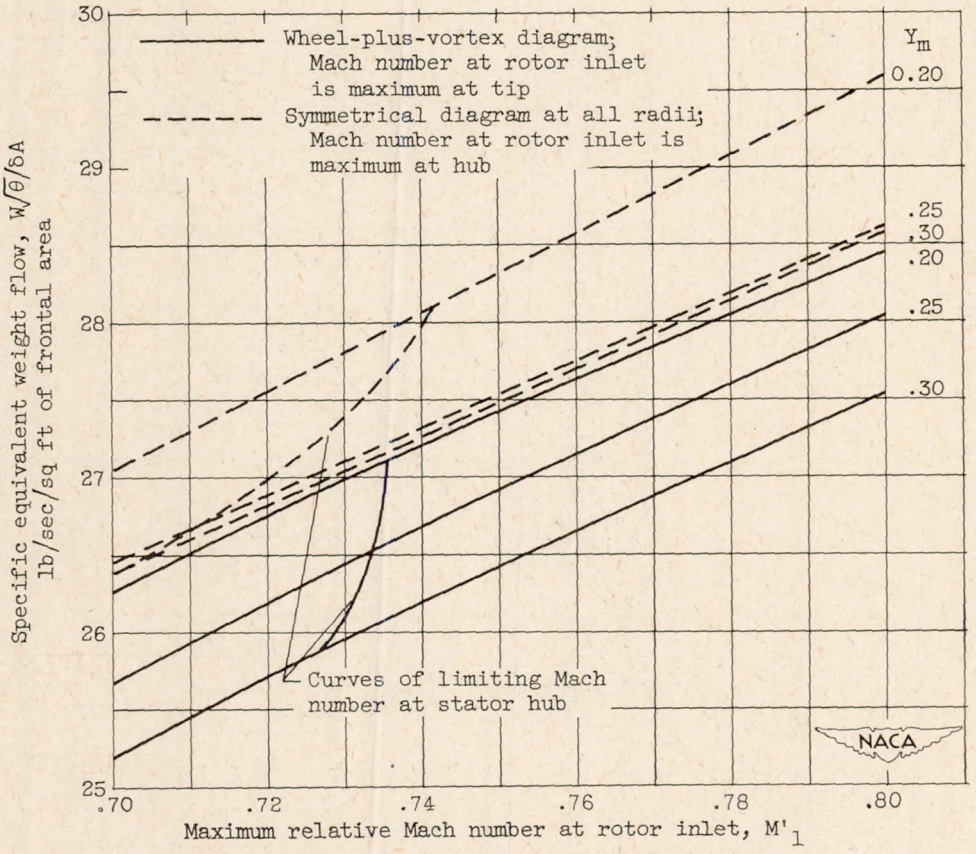


(b) Specific equivalent weight flow.

Figure 2. - Continued. Operating conditions of inlet stage. Hub-to-tip ratio, 0.5; rotor-tip relative inlet-air angle, 55°.

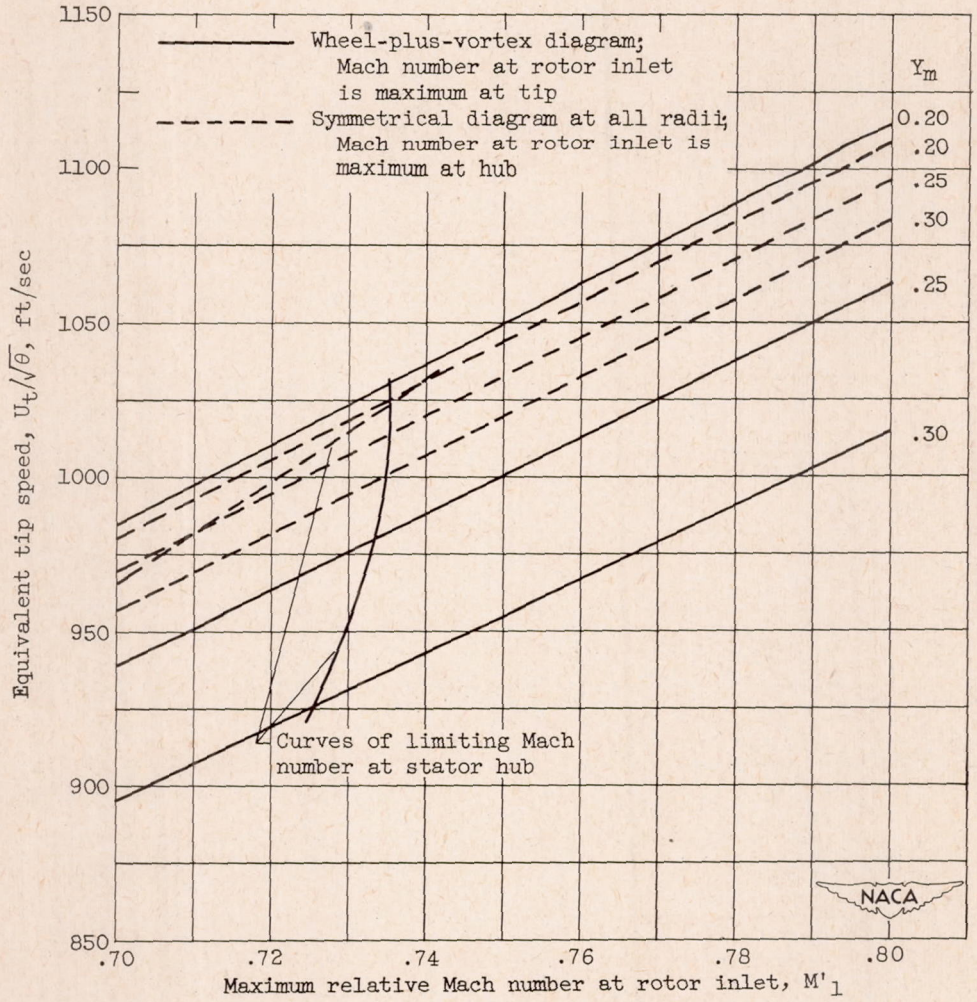


(c) Equivalent tip speed.

Figure 2. - Continued. Operating conditions of inlet stage. Hub-to-tip ratio, 0.5; rotor-tip relative inlet-air angle, 55°.

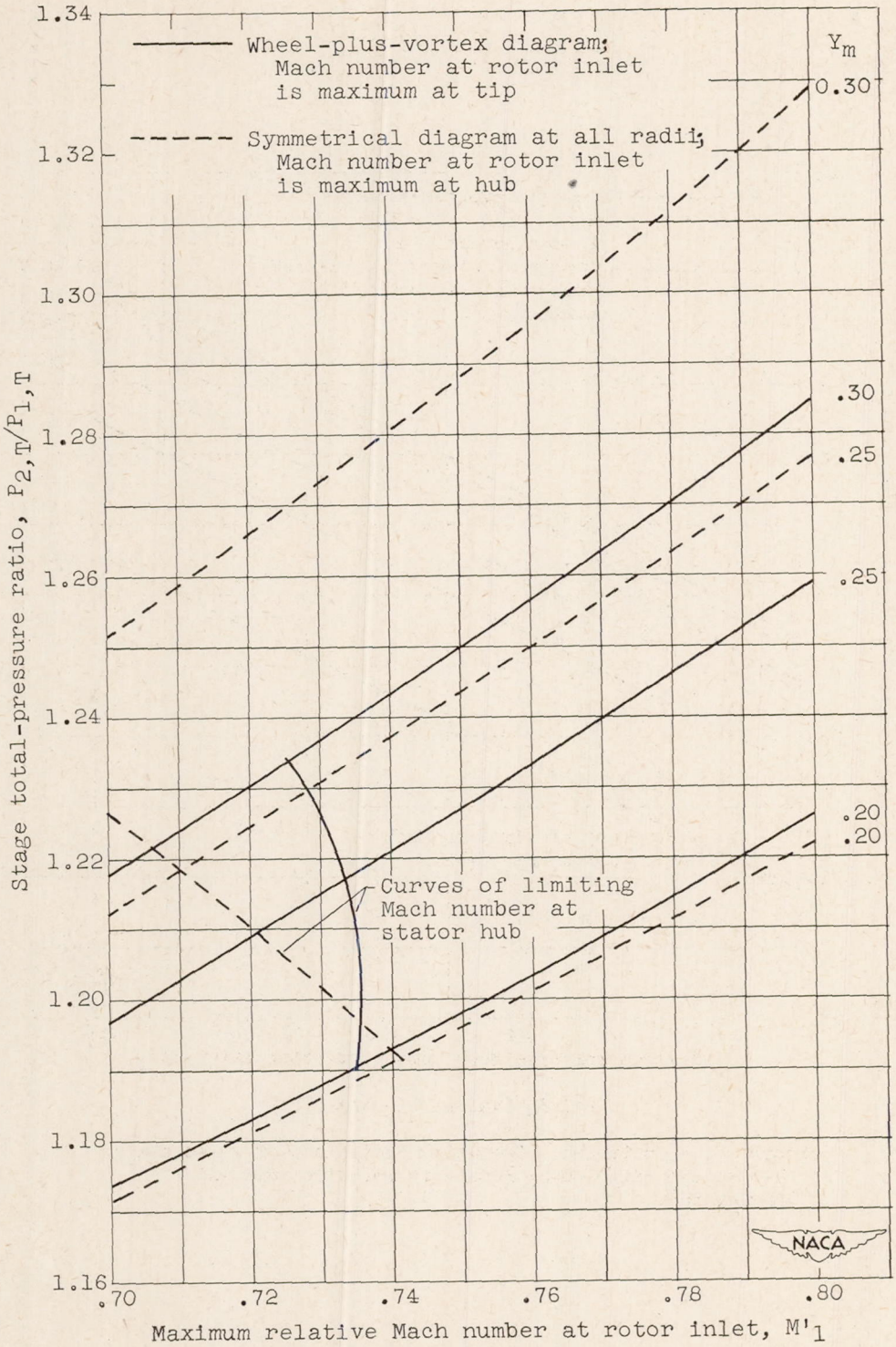


(d) Stage total-pressure ratio.

Figure 2. - Concluded. Operating conditions of inlet stage. Hub-to-tip ratio, 0.5; rotor-tip relative inlet-air angle, 55°.

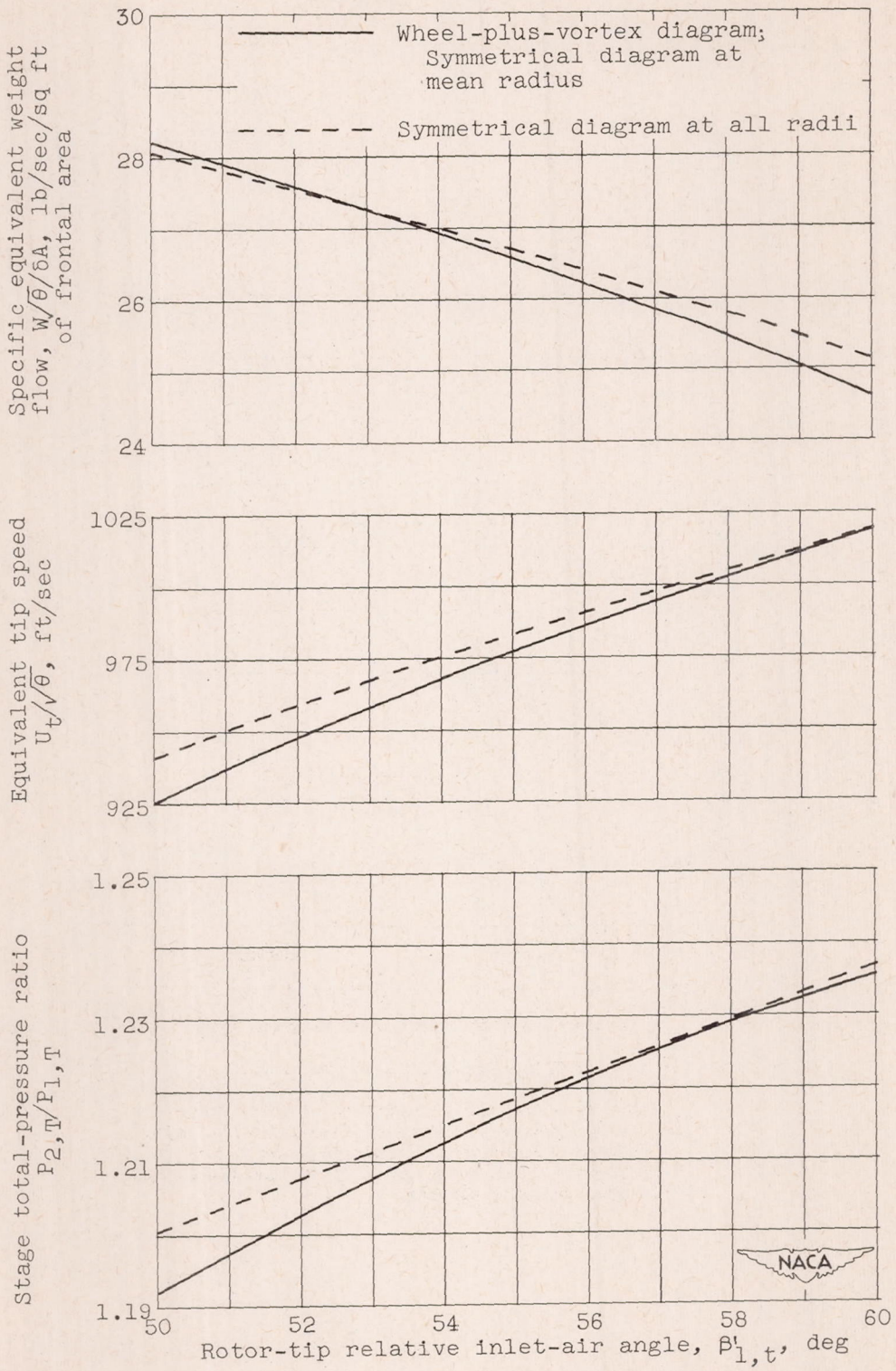


Figure 3. - Variation of operating conditions with rotor-tip relative inlet-air angle. Limiting Mach number at stator hub; $Y_m$, 0.25.

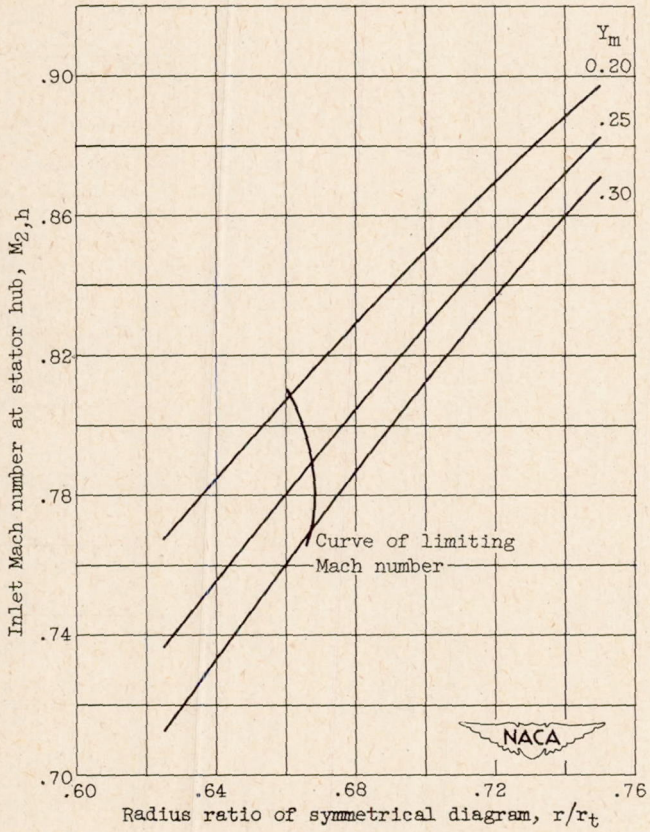


(a) Inlet Mach number at stator hub.

Figure 4. - Operating conditions of inlet stage for various radial positions of symmetrical velocity diagram. Relative inlet-air angle at rotor tip, 60°; rotor-tip inlet Mach number, 0.80; and wheel-plus-vortex velocity diagram.

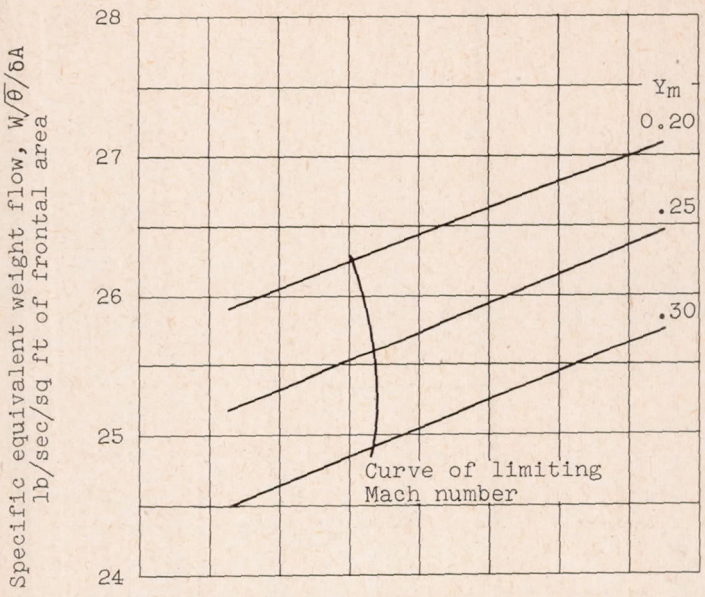


(b) Specific equivalent weight flow.

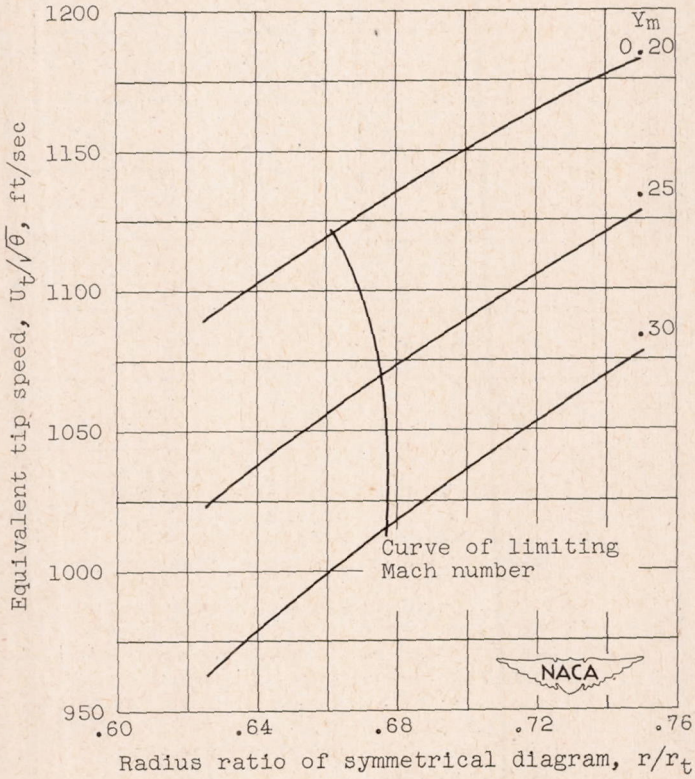


(c) Equivalent tip speed.

Figure 4. - Continued. Operating conditions of inlet stage for various radial positions of symmetrical velocity diagram. Relative inlet-air angle at rotor tip, 60°; rotor-tip inlet Mach number, 0.80; and wheel-plus-vortex velocity diagram.

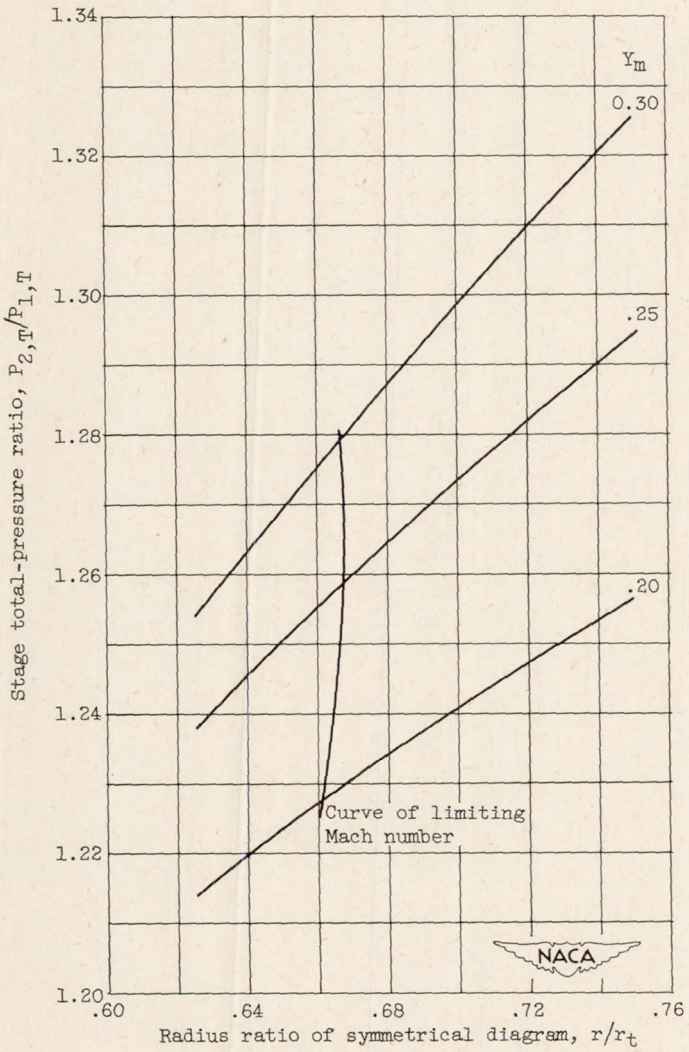


(d) Stage total-pressure ratio.

Figure 4. - Concluded. Operating conditions of inlet stage for various radial positions of symmetrical velocity diagram. Relative inlet-air angle at rotor tip, 60°; rotor-tip inlet Mach number, 0.80; and wheel-plus-vortex velocity diagram.

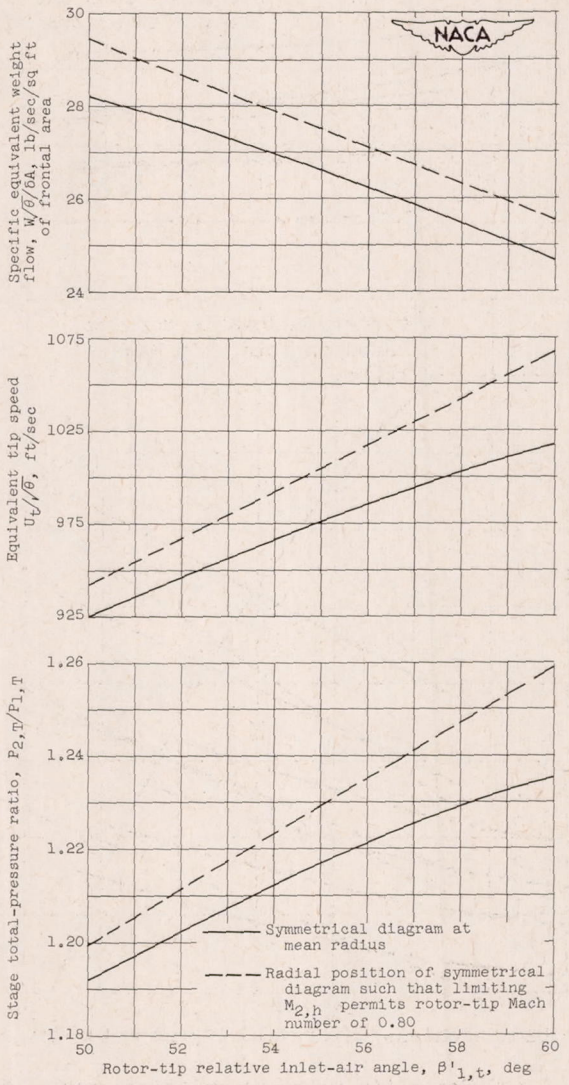


Figure 5. - Variation of operating conditions with relative inlet-air angle. Limiting Mach number at stator hub; $Y_m$, 0.25; and wheel-plus-vortex diagram.

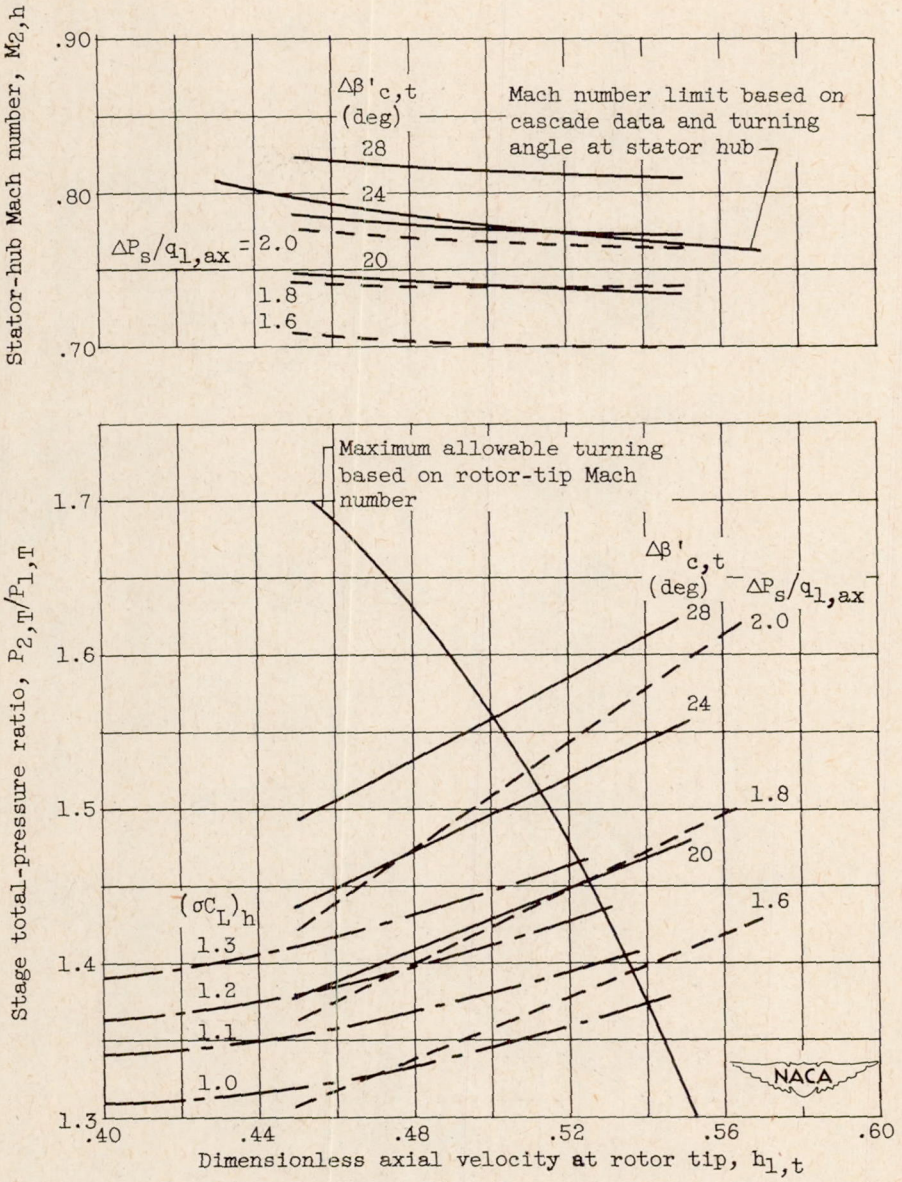


(a) Rotor-tip relative inlet-air angle, 55°.

Figure 6. - Variation of operating conditions with dimensionless axial velocity for various limiting conditions in intermediate stage. Over-all total-pressure ratio, 3.0.

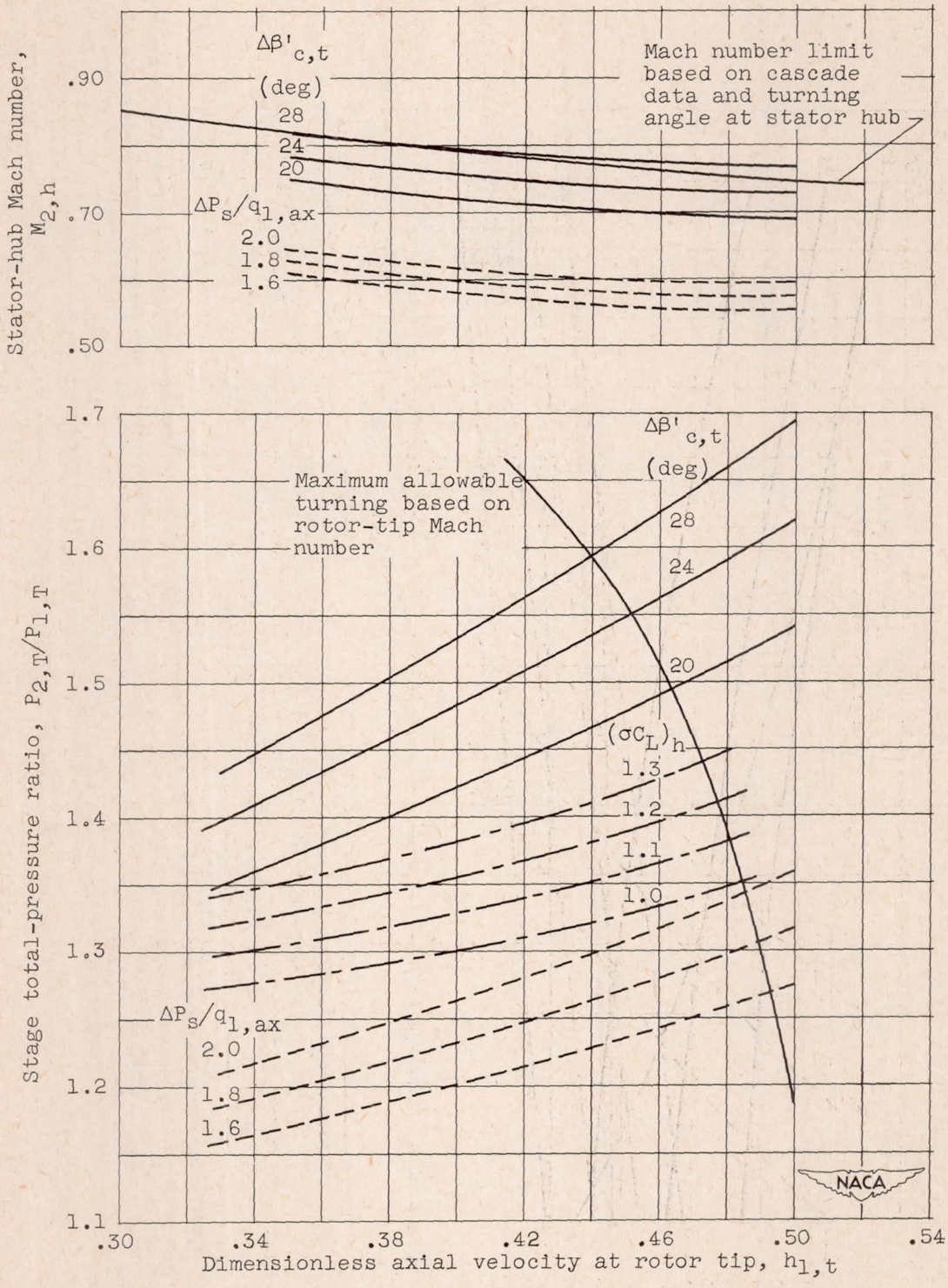


(b) Rotor-tip relative inlet-air angle, $60^\circ$.

Figure 6. - Concluded. Variation of operating conditions with dimensionless axial velocity for various limiting conditions in intermediate stage. Over-all total-pressure ratio, 3.0.

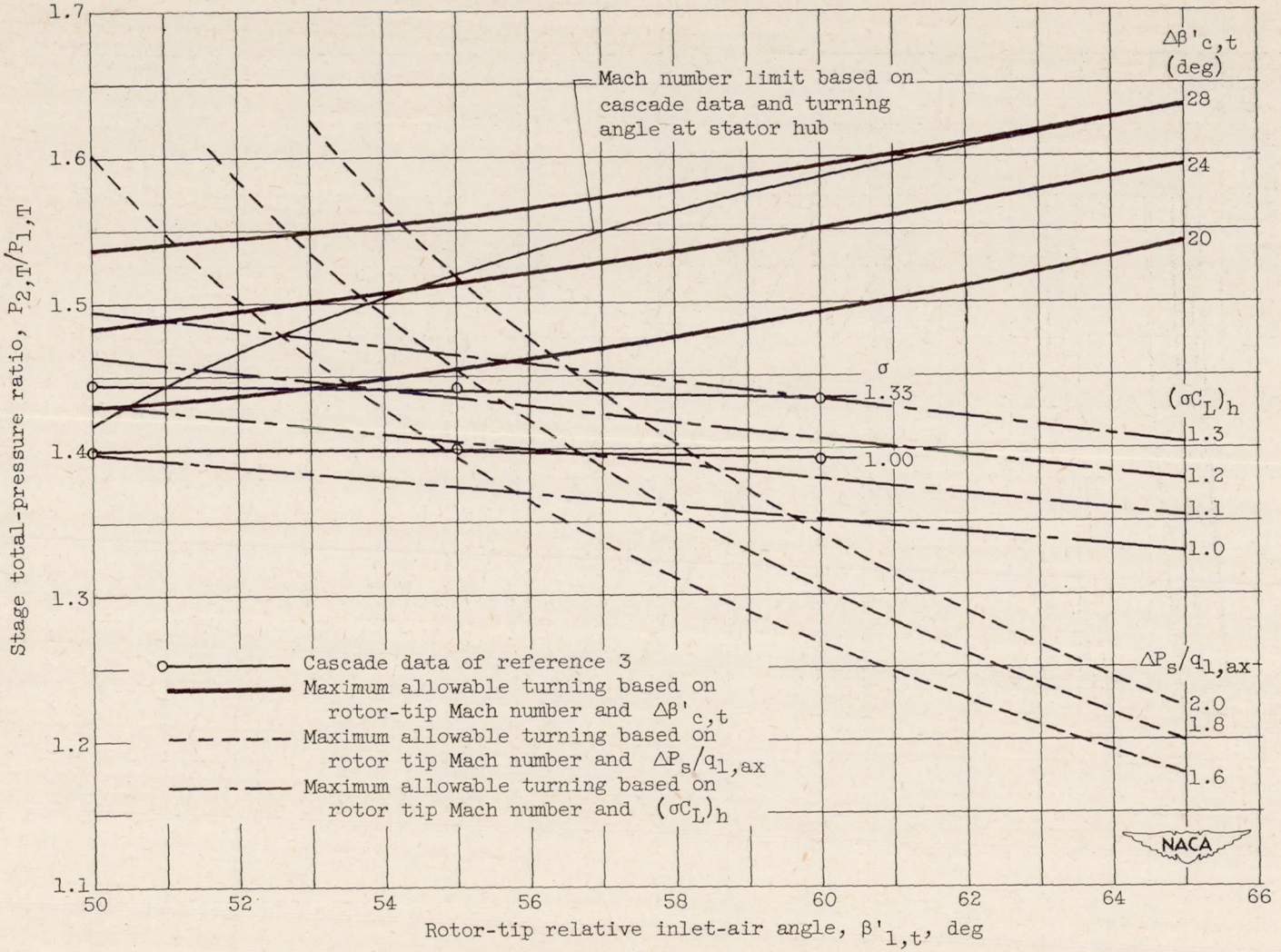


(a) Stage total-pressure ratio.

Figure 7. - Variation of operating conditions with rotor-tip relative inlet-air angle for various limiting conditions in intermediate stage. Over-all total-pressure ratio, 3.0.

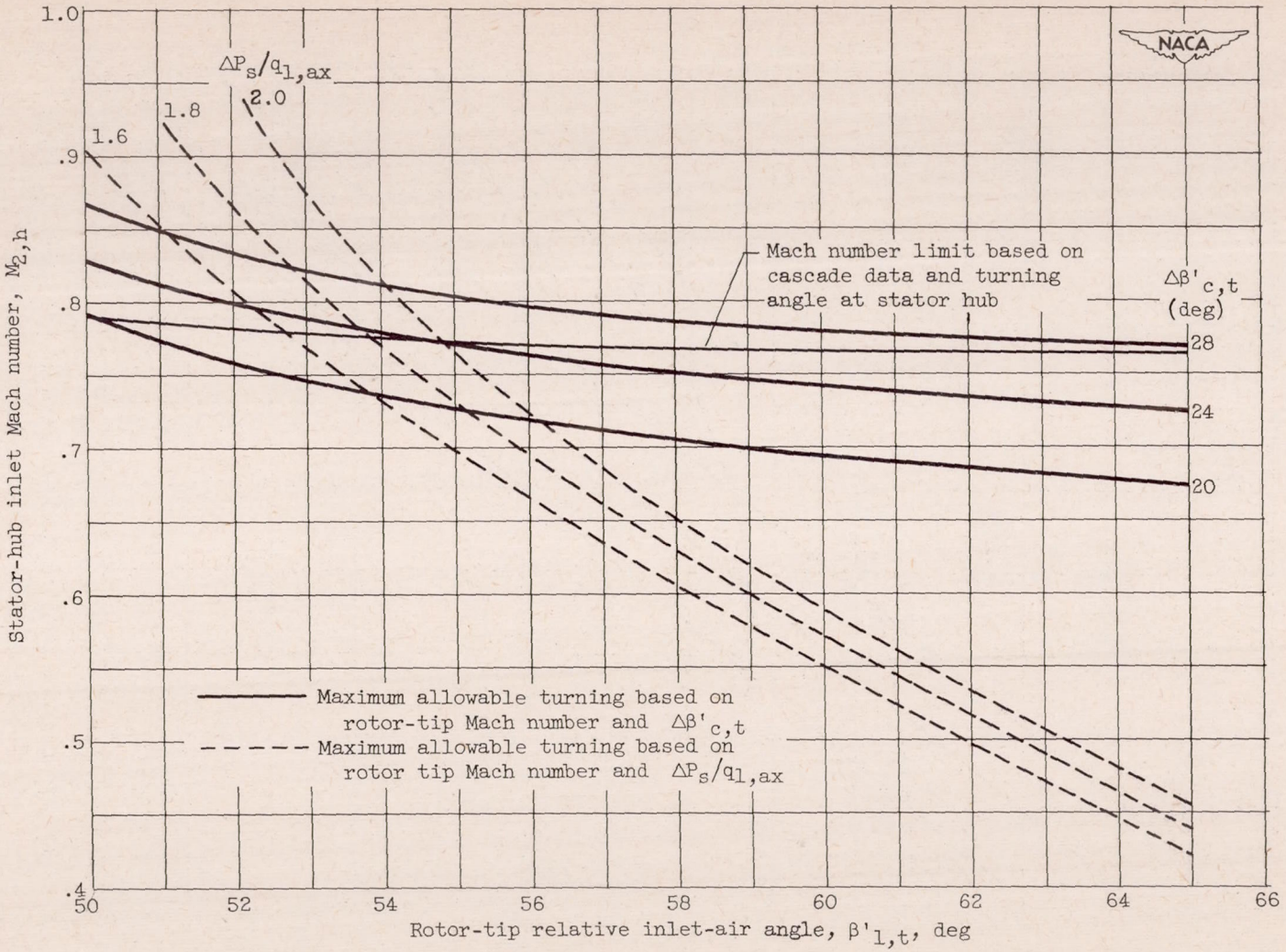


(b) Stator-hub inlet Mach number.

Figure 7. - Concluded. Variation of operating conditions with rotor-tip relative inlet-air angle for various limiting conditions in intermediate stage. Over-all total-pressure ratio, 3.0.

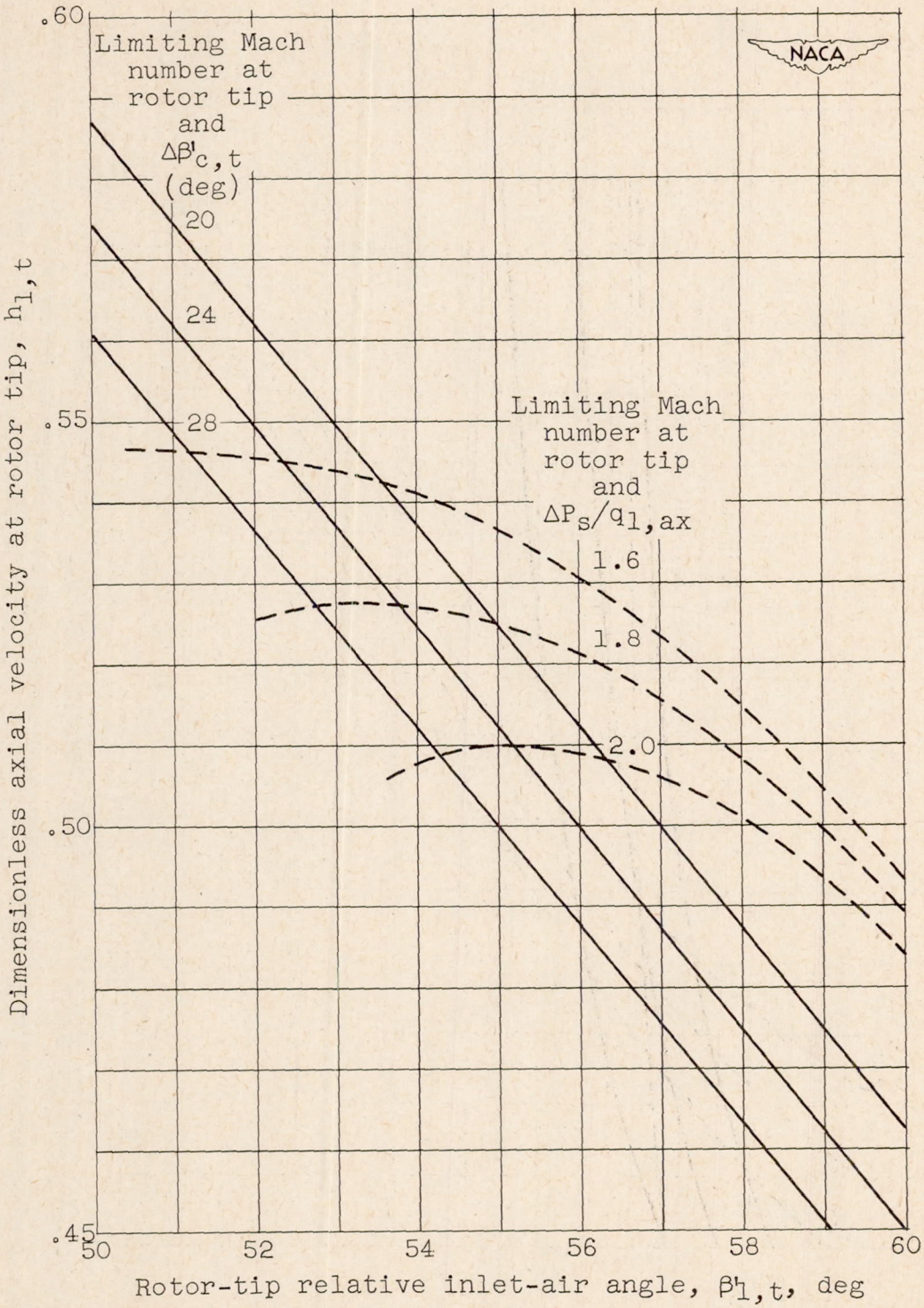


Figure 8. - Variation of dimensionless axial-velocity ratio at rotor tip with relative inlet-air angle for various limiting conditions in intermediate stage. Over-all total-pressure ratio, 3.0.

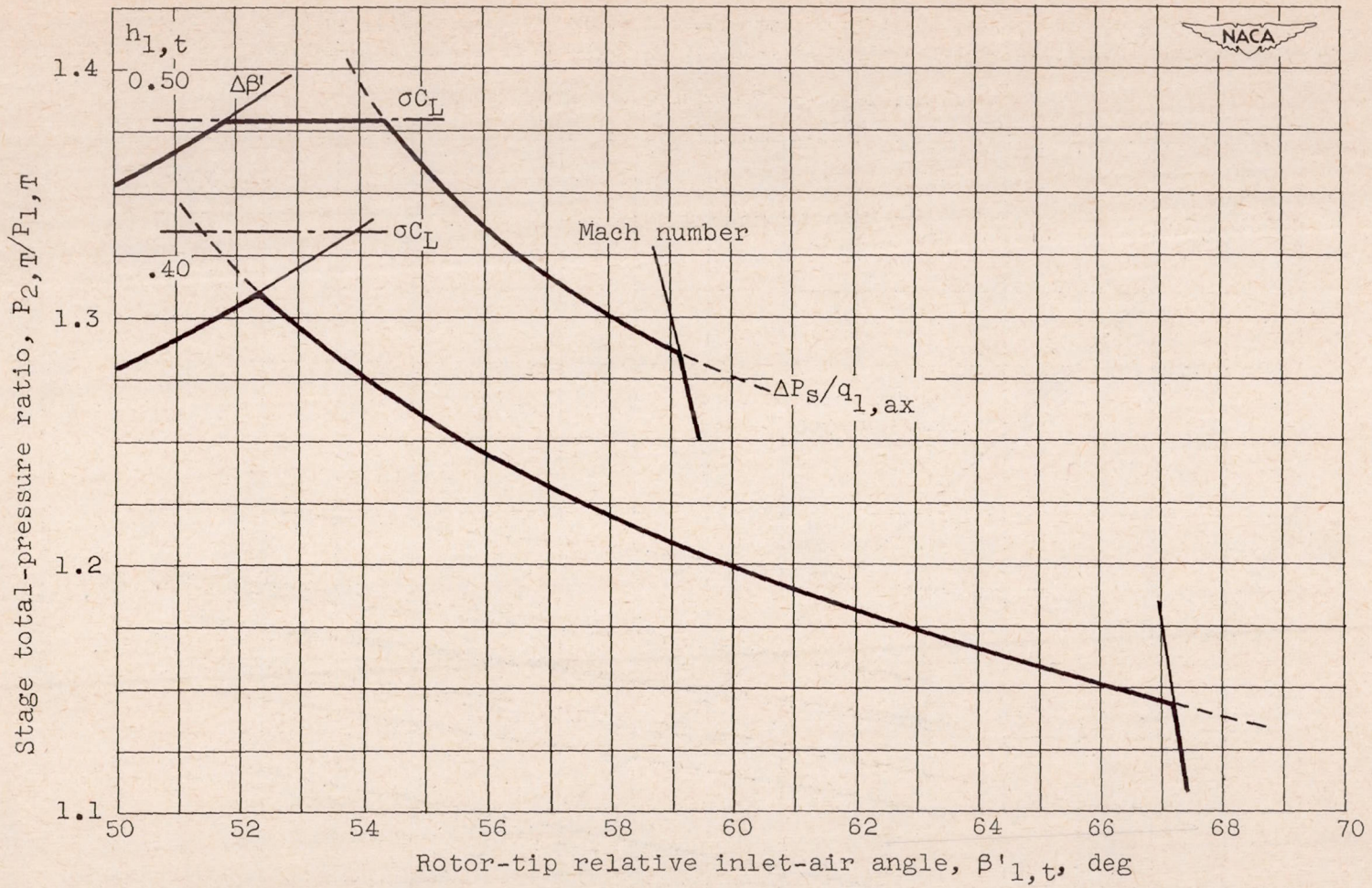


Figure 9. - Variation of stage total-pressure ratio with rotor-tip relative inlet-air angle for two dimensionless axial velocities and given set of limiting conditions in intermediate stage. Over-all total-pressure ratio at stage inlet, 3.0. Limiting conditions: $\Delta\beta'_{c,t}$, 20°; $(\sigma C_L)_h$, 1.1; $\Delta P_s/q_{1,ax}$, 1.6; Mach number, f(turning).

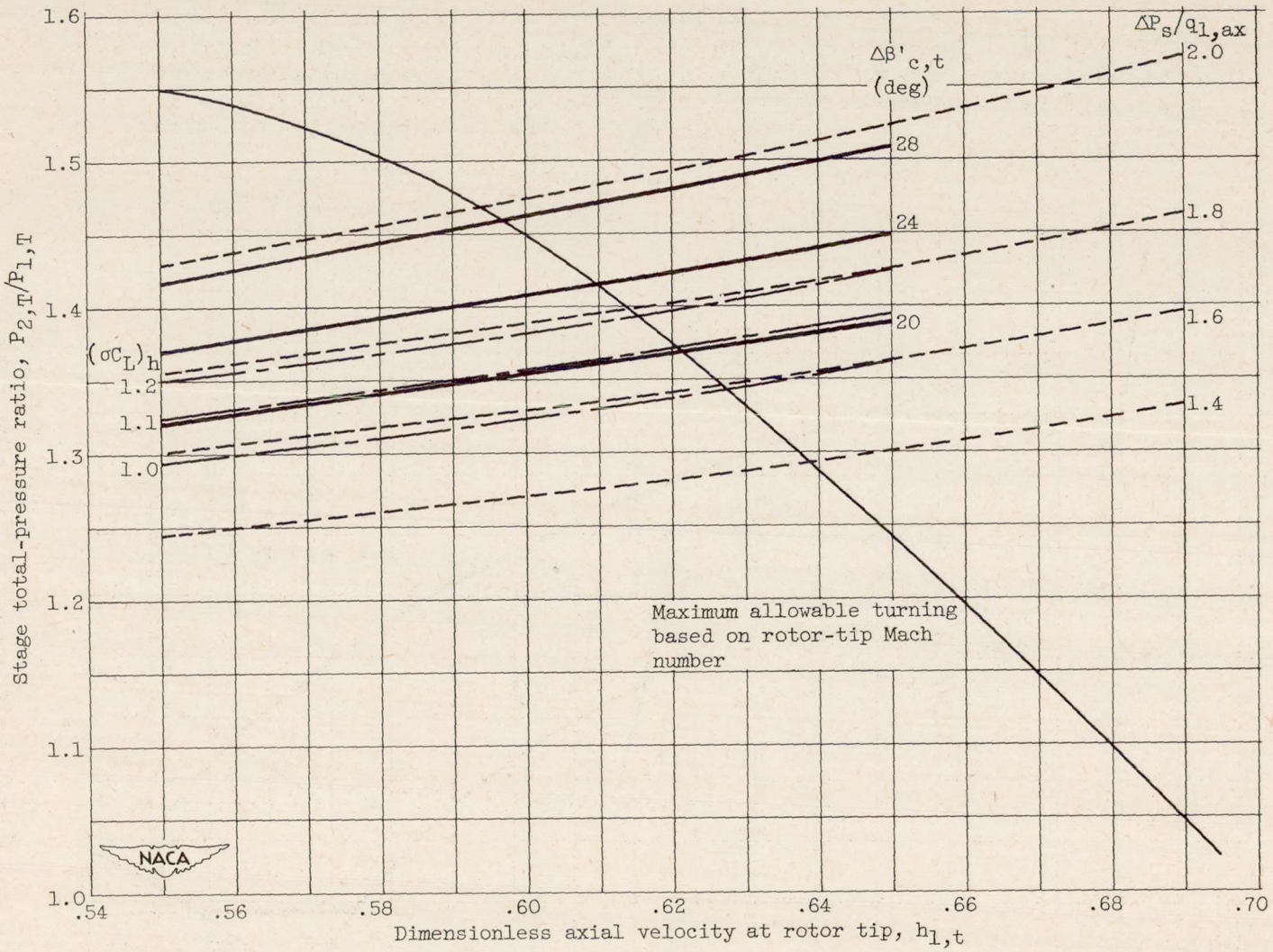


Figure 10. - Variation of operating conditions with dimensionless axial velocity for various limiting conditions in final stage. Over-all total-pressure ratio, 9.0; relative inlet-air angle at rotor tip, 55°.

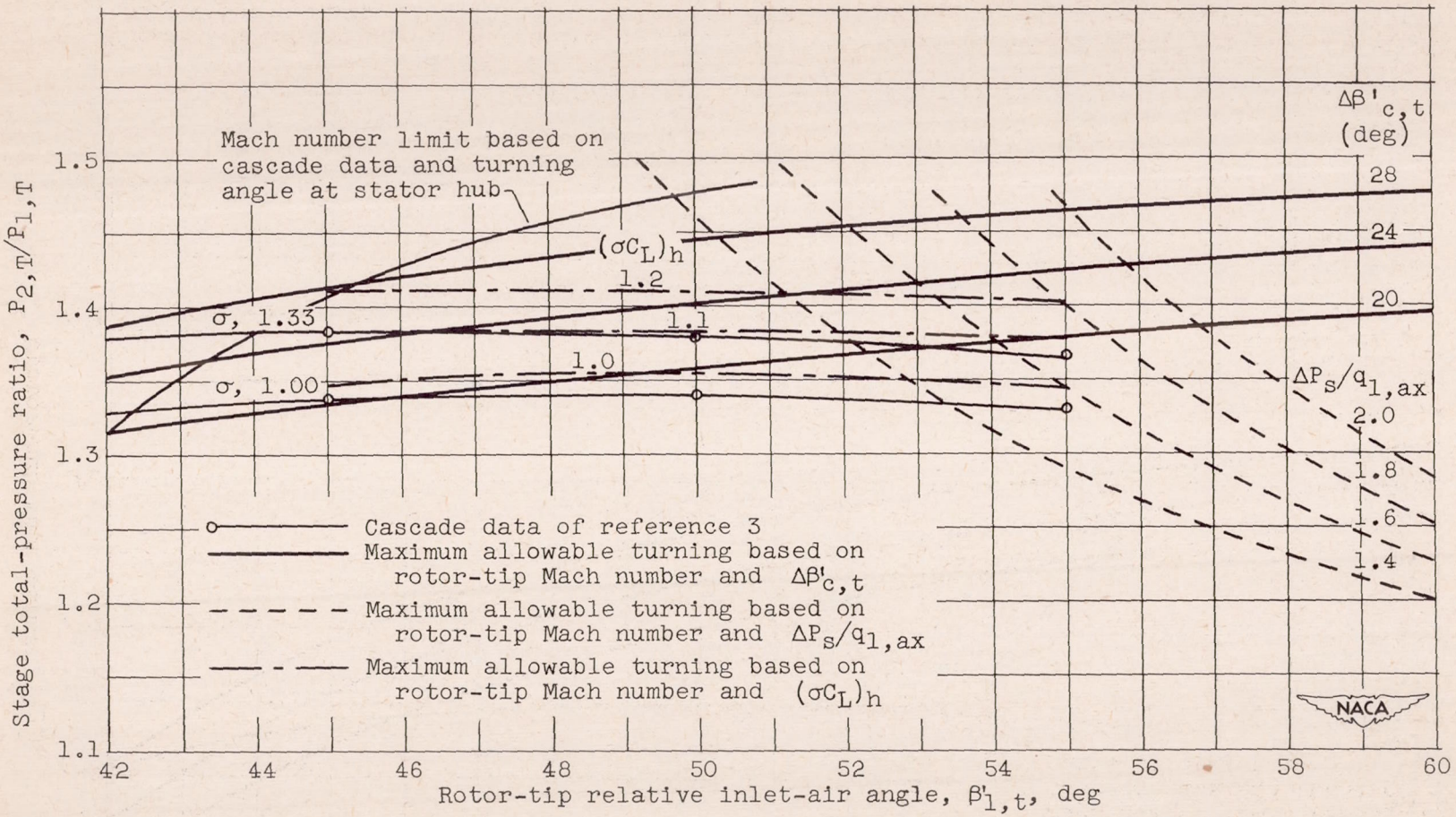


(a) Stage total-pressure ratio.

Figure 11. - Variation of operating conditions with rotor-tip relative inlet-air angle for various limiting conditions in final stage. Over-all total-pressure ratio, 9.0.

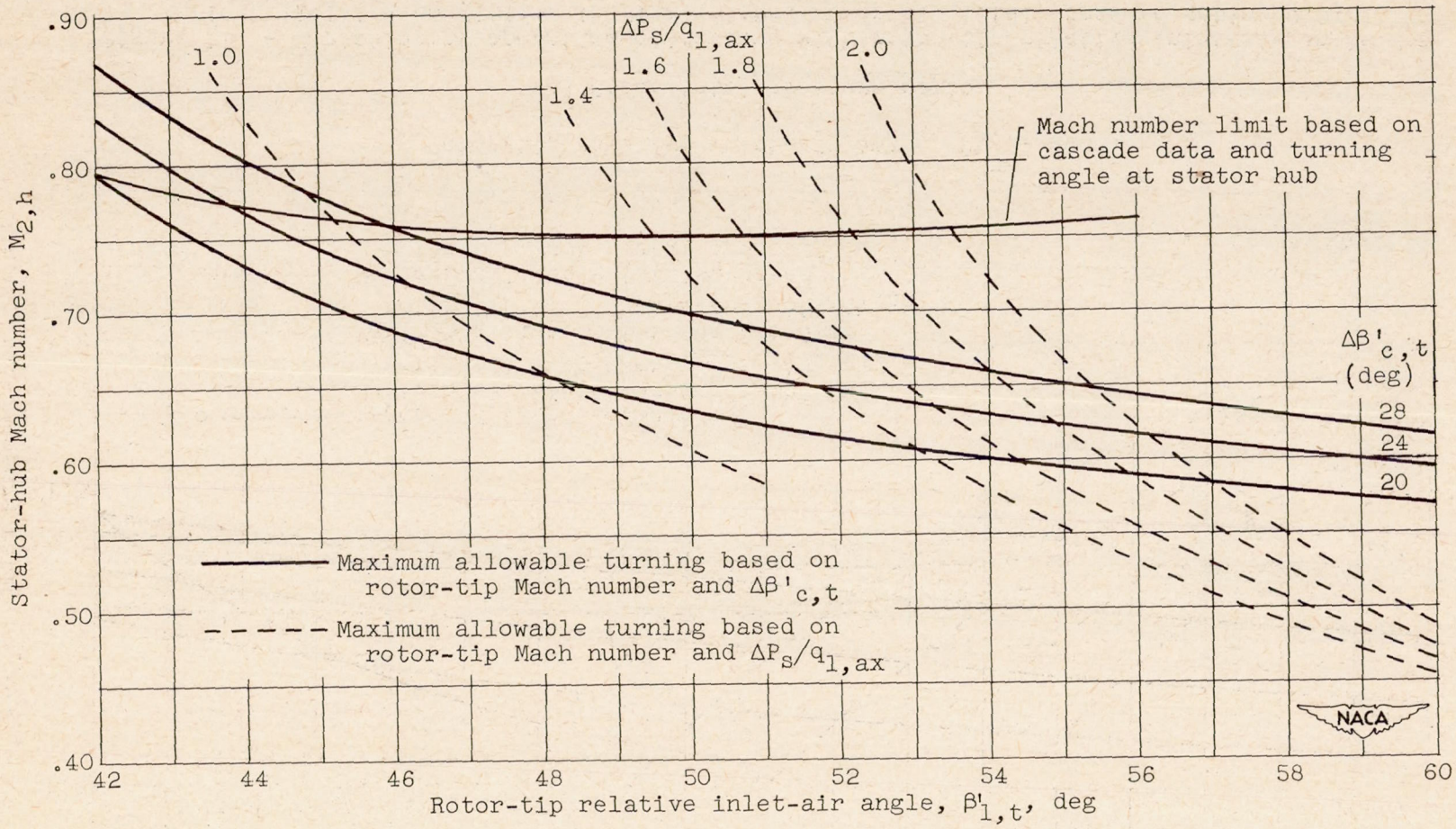


(b) Stator-hub entrance Mach number.

Figure 11. - Concluded. Variation of operating conditions with rotor-tip relative inlet-air angle for various limiting conditions in final stage. Over-all total-pressure ratio, 9.0.

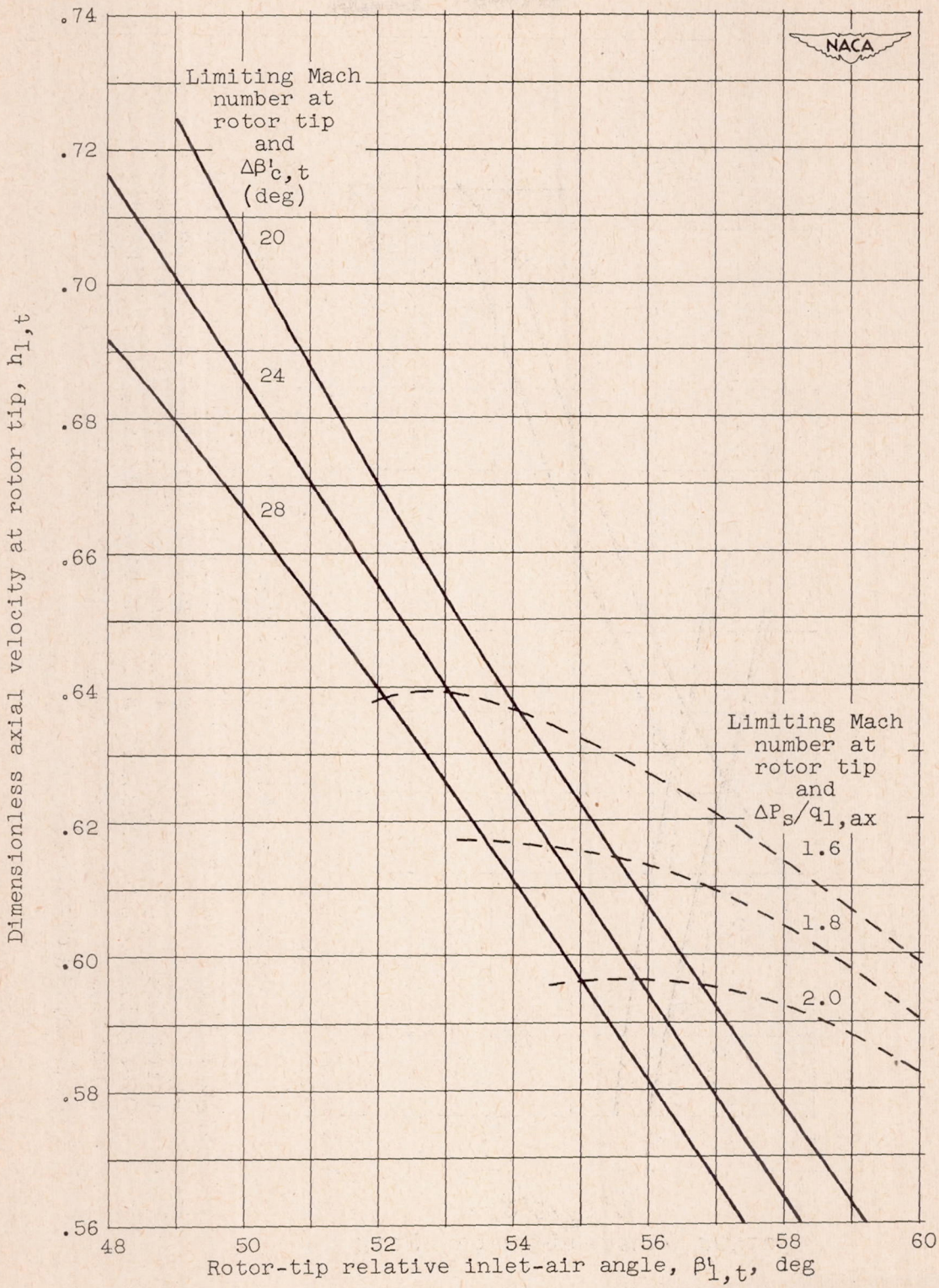


Figure 12. - Variation of dimensionless axial velocity at rotor tip with inlet-air angle for several limiting conditions in final stage. Over-all total-pressure ratio, 9.0.

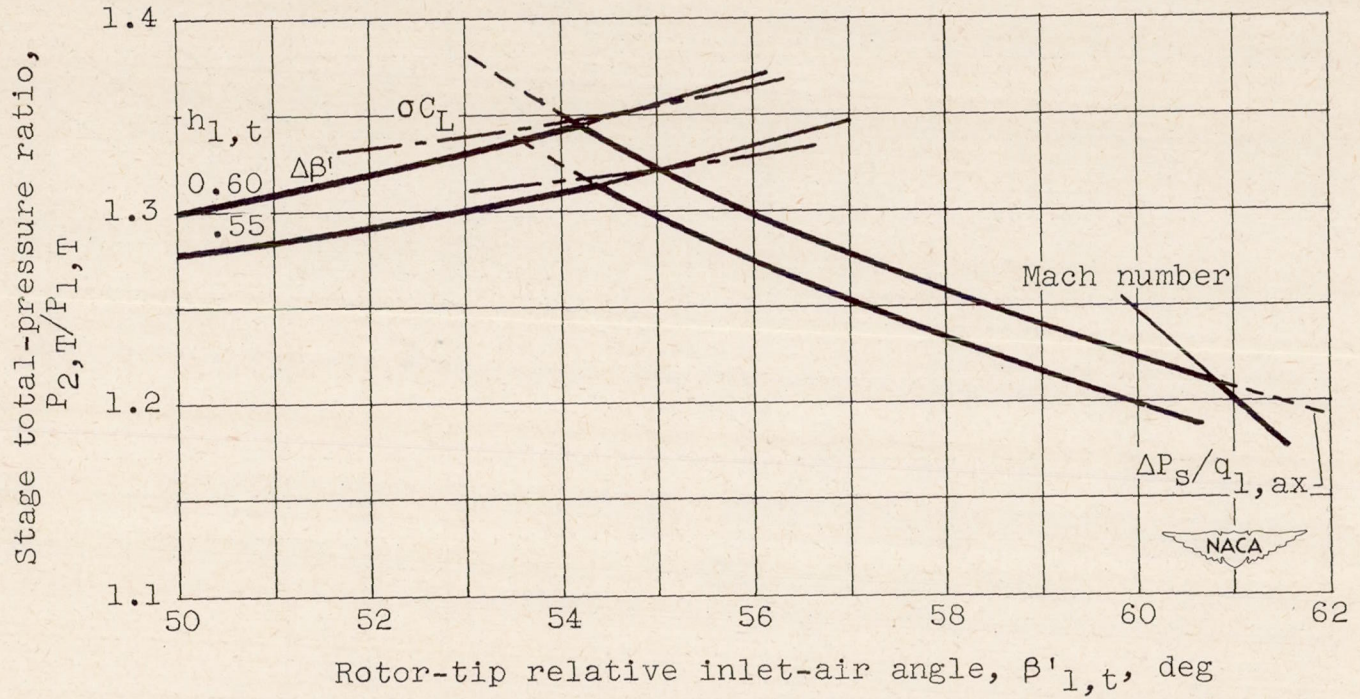


Figure 13. - Variation of stage total-pressure ratio with rotor-tip relative inlet-air angle for two dimensionless axial velocities and a given set of limiting conditions in final stage. Over-all total-pressure ratio at stage inlet, 9.0. Limiting conditions: $\Delta\beta'_{c,t}$, 20°; $(\sigma C_L)_h$, 1.1; $\Delta P_s/q_{1,ax}$, 1.6; Mach number, f(turning).

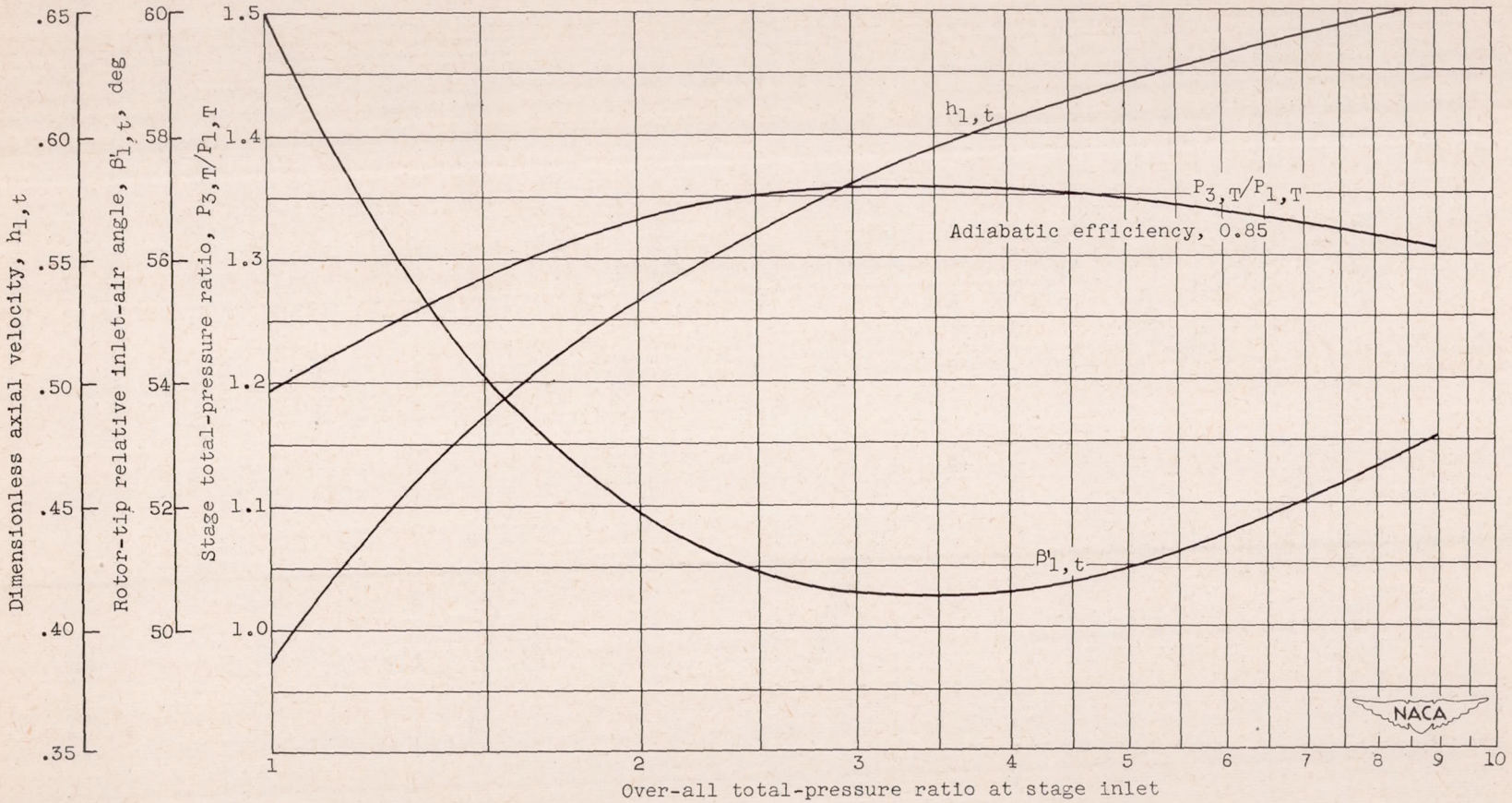


Figure 14. - Variation of dimensionless axial velocity at rotor tip, rotor-tip relative inlet-air angle, and stage total-pressure ratio with over-all total-pressure ratio at the stage inlet. Limiting conditions: $\Delta\beta'_{c,t}$, 20°; $(\sigma C_L)_h$, 1.1; $\Delta P_s/q_{1,ax}$, 1.6; Mach number, f(turning).

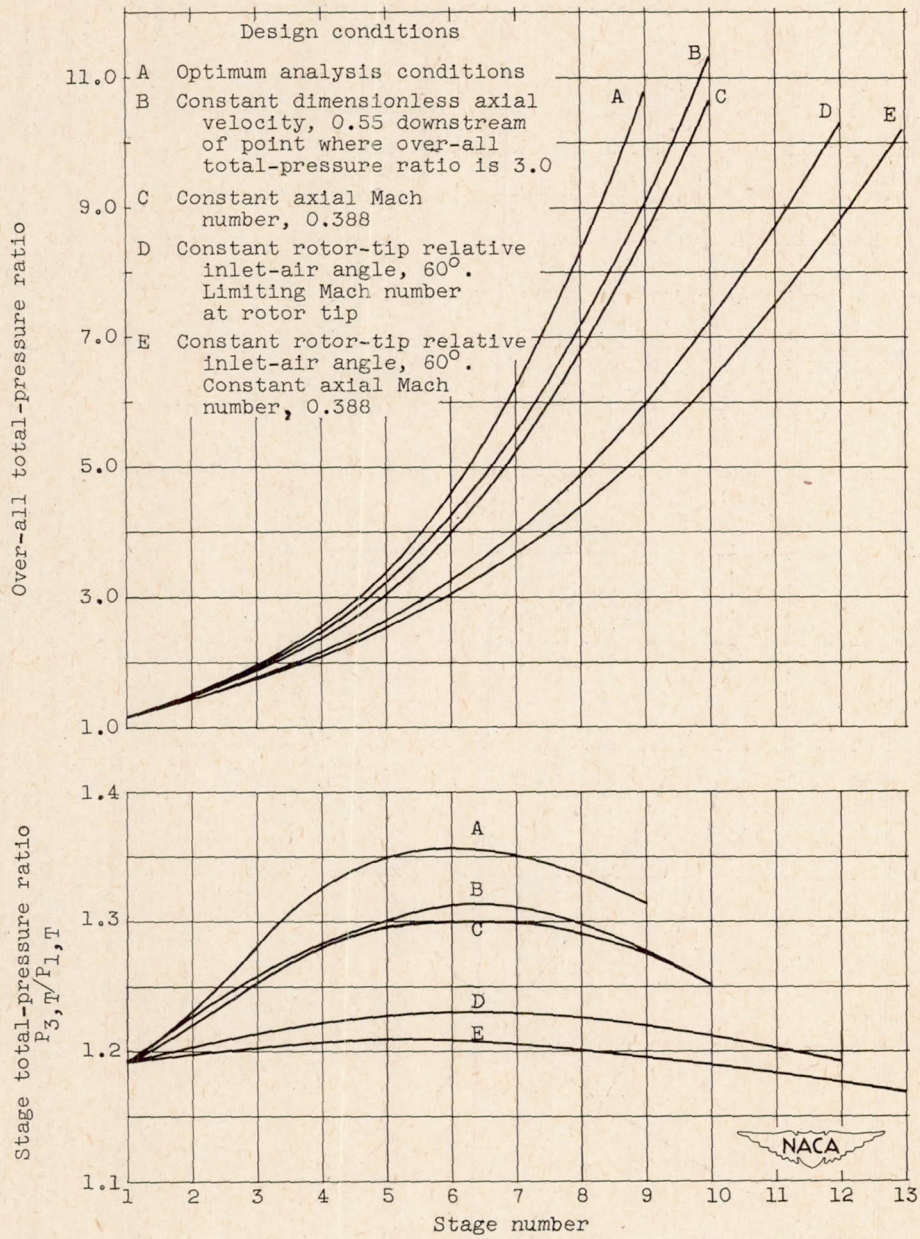


(a) At stage outlet.

Figure 15. - Operating conditions through multistage compressor for various design conditions. Limiting conditions: $\Delta\beta'_{c,t}$, 20°; $(\sigma C_L)_h$, 1.1; $\Delta P_s/q_{1,ax}$, 1.6; Mach number, f(turning).

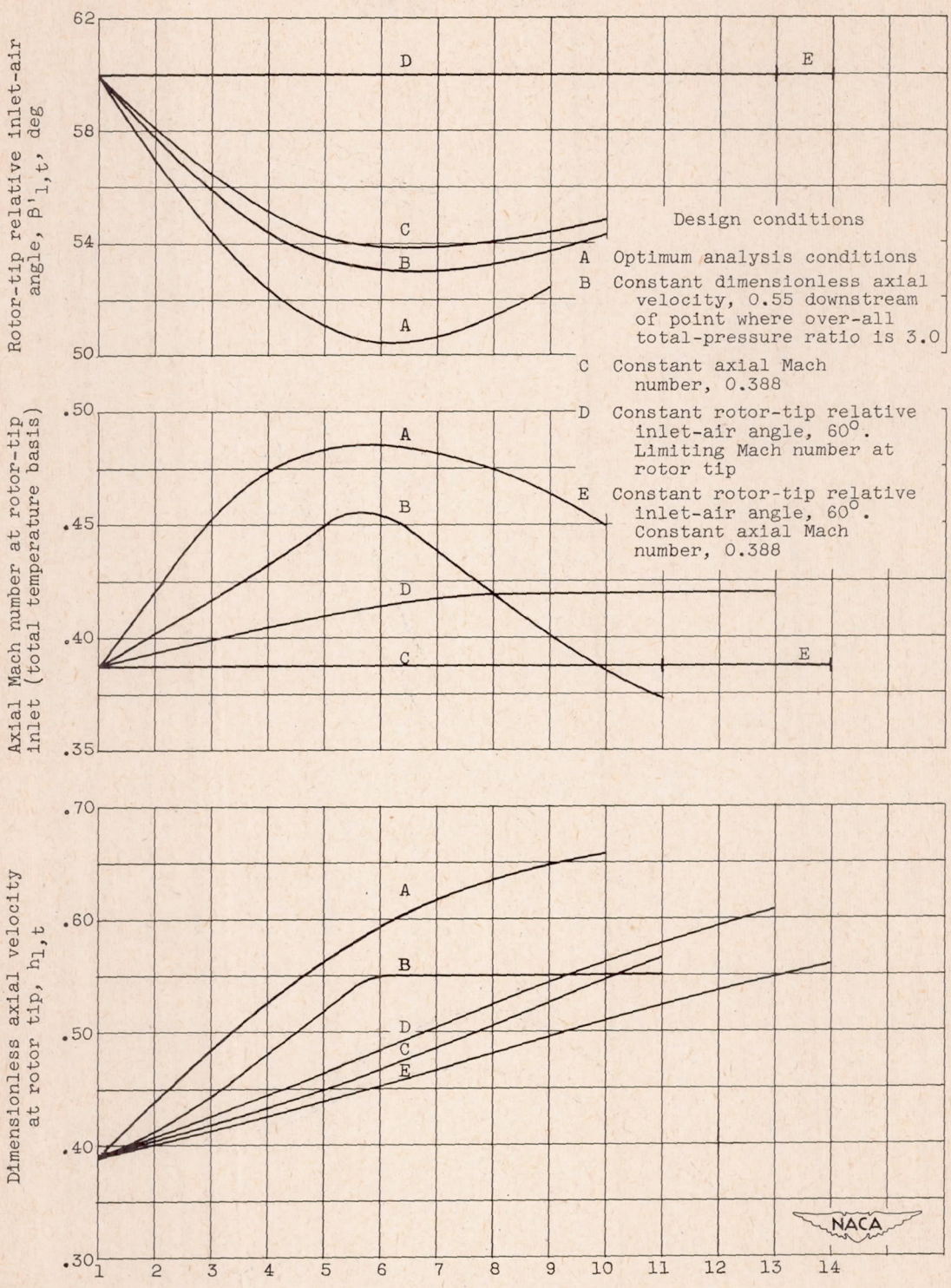


(b) At stage inlet.

Figure 15. - Concluded. Operating conditions through multistage compressor for various design conditions. Limiting conditions: $\Delta\beta'_{c,t}$, 20°; $(\sigma C_L)_h$, 1.1; $\Delta P_s/q_{1,ax}$, 1.6; Mach number, f(turning).

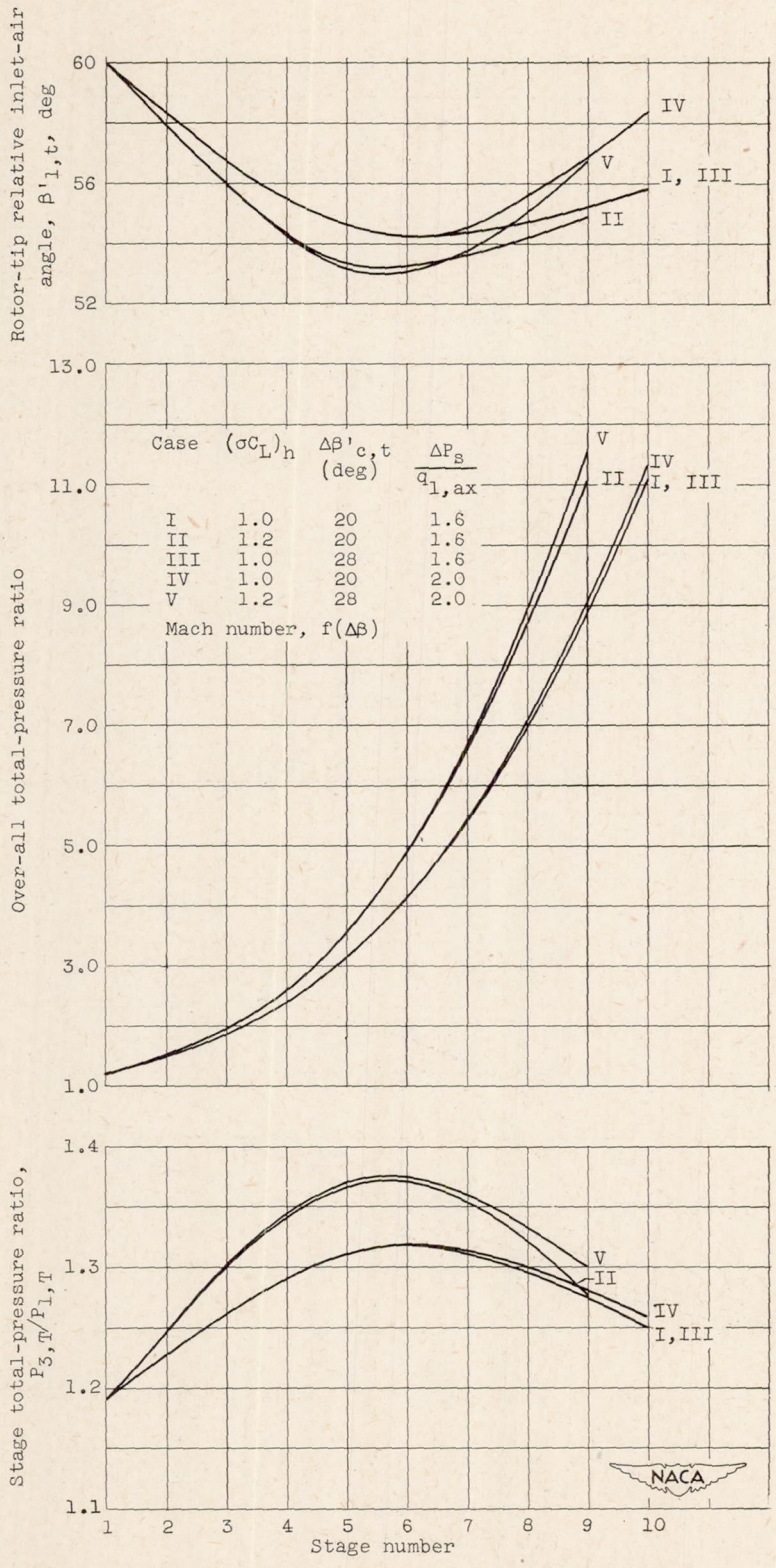


Figure 16. - Operating conditions through multistage compressor having constant dimensionless axial velocity at rotor tip of 0.55 downstream of point where over-all total-pressure ratio is 3.0 for several limiting conditions.